2010

Near infrared photovoltaic micro-cell for optical fibre based power harvesting

Gary Allwood
Edith Cowan University

Edith Cowan University

Copyright Warning

NEAR INFRARED PHOTOVOLTAIC MICRO-CELL FOR OPTICAL FIBRE BASED POWER HARVESTING

Gary Allwood
Bachelor of Science (Physics and Mathematics), ECU, 2007

Bachelor of Science Honours (Physics) Thesis

School of Engineering
Faculty of Computing, Health and Science
Edith Cowan University

October 2010

USE OF THESIS

The Use of Thesis statement is not included in this version of the thesis.

ABSTRACT

A photonic power system using a silicon or germanium based device as a photonic power converter was proposed. The properties of each device were investigated to determine the optimum structure, design, configuration and efficiency for power conversion. These included, but were not limited to, device geometry, doping concentration and the wavelength of the incident beam. Relevant inferences were made from the results obtained and compared to previous work.

Currently, research into photovoltaic power converters is focused on the efficiencies of complex heterostuctures made from gallium-arsenide compounds. Here, the properties of a silicon device were investigated in detail as the predicted efficiency under monochromatic light is comparatively high, much more than solar generated power, which will therefore reduce the cost of optically powered systems.

The results show that an optimised silicon based photovoltaic micro-cell can produce optical to electrical power conversion as high as 43% under illumination of 980nm light. We have shown that the wavelength of the incident light determines the depth of the optimised device. The peak doping concentrations of the emitter and base regions should be as high as $1x10^{20}cm^{-3}$ and $3x10^{17}cm^{-3}$, respectively, for maximum power conversion efficiency. The results also show that germanium-based homojunction cells can produce power conversion efficiencies as high as 36% when illuminated by 1550nm light.

The validity of a completely optical network is discussed, as experiments with multiple sources propagating along a single optical fibre have been performed. Three separate signals, one for communication, one for sensing and one for power generation, can utilise the same optical fibre will no significant loss to information or power.

This research is the basis for a more comprehensive study of the highest attainable efficiency of a silicon photovoltaic power converter under illumination of monochromatic light and the feasibility of a completely photonic network.

DECLARATION

I certify that this thesis does not, to the best of my knowledge and belief:

(i) incorporate without acknowledgment any material previously submitted for a degree or diploma in any institution of higher education.

(ii) contain any material previously published or written by another person except where due reference is made in the text; or

(iii) contain any defamatory material.

I also grant permission for the Library at Edith Cowan University to make duplicate copies of my thesis as required.

Signature: ... .

Date: ....14.3.11.....

ACKNOWLEDGEMENTS

I wish to acknowledge the ongoing support from my supervisor Associate Professor Steven Hinckley, my assistant supervisor Dr Graham Wild and Mr Paul Jansz for taking the time to answer any questions I have presented them with, as well as their continued assistance when required.

TABLE OF CONTENTS

LIST OF PUBLICATIONS

1. G. Allwood, G. Wild and S. Hinckley, "Photovoltaic Micro-Cell Design for Distributed Power in Sensor Networks," proceedings of the 2010 Conference on Optoelectronic and Microelectronic Materials and Devices (COMMAD).

2. G. Allwood, G. Wild and S. Hinckley, "Photovoltaic Micro-Cell Design for Distributed Power-over-Fibre Optimized for 850nm & 980nm," proceedings of the 19th Australian Institute of Physics (AIP) Congress 2010.

3. G. Allwood, G. Wild and S. Hinckley, "Power Over Fibre: Material Properties of Homojunction Photovoltaic Micro-Cells," proceedings of the 6th International Symposium on Electronic Design, Test and Applications (DELTA) 2011.

4. G. Allwood, G. Wild and S. Hinckley, "Power-over-Fibre for Distributed Optical Fibre Smart Sensor Networks," proceedings of the 35th Australian Conference on Optical Fibre Technology (ACOFT) 2010.

5. G. Wild, G. Allwood and S. Hinckley, "Distributed Sensing, Communications, and Power in Optical Fibre Smart Sensor Networks for Structural Health Monitoring," proceedings of the 2010 6th International Conference on Intelligent Sensors, Sensor Networks and Information Processing (ISSNIP).

CHAPTER 1

INTRODUCTION

In this chapter, an overview of the project is given, along with a relevant background to power over fibre and the development of photovoltaic power converters. The main aim, significance, status and problems associated with the project are also discussed, and the chapter concludes with the objectives and research questions.

1.1. Overview

Research into the optical and electrical properties of silicon and germanium for device physics has progressed immensely over the last few decades. The applications of solid state physics are now extremely broad and affect most people in western society on a day-to-day basis. Albeit, silicon is well known to be a poor semiconductor with respect to many of its applications, including solar cells and other types of diodes, however, because of its abundance and relatively cheap fabricating costs, it has dominated many industries as the main source of manufacturing material. In recent years many exciting applications have arisen from research in to the properties of more complex compounds, such as high powered laser diodes and thin film solar cells, however, silicon is still the most viable solution for most applications because of cost.

In this paper, we suggest a novel idea of coupling a silicon photodiode to an optical fibre to be used as a photovoltaic power converter (PPC) for use in optical fibre networks. Although silicon is not the most efficient optical power converter, it is suitable for specific applications. Silicon has a relatively high bandgap energy of 1.12eV and therefore operates as a PPC in the region between 300nm and 1100nm, with an optimum wavelength of 850nm in terms of its responsivity, the ratio of electrical output to optical input. This wavelength is particularly useful as the attenuation in an optical fibre is minimal. Attenuation is also minimal at wavelengths of 1310nm and 1550nm, which are commonly used for transmitting communication signals. This means a power signal launched into an optical fibre to be detected by a

silicon photodiode would not interfere with a communication signal transferred down the fibre. Moreover, the PPC could be placed in front of the communication module, as it would be transparent to the communication signal. This configuration would therefore require no splitting of the two signals. The main motivation behind this research is to investigate what properties of a silicon photovoltaic cell restrict the maximum output power and whether enough power can be generated to efficiently power a device using a monochromatic light source over an optical fibre.

1.2. Background

The goal of this project is to investigate the properties of a photonic power system in order to optimize its efficiency as a photovoltaic micro-cell under monochromatic illumination. A brief background of this concept is given in the following section.

Photonics, as defined by the United States National Research Council, is "the field of science and engineering encompassing the physical phenomena and technologies associated with the generation, transmission, manipulation, detection, and utilization of light", [1]. This research is primarily focused on the generation of photonic power for low powered microelectronics.

The photoelectric effect was discovered in 1839 by French physicist Alexandre-Edmond Becquerel, although its properties were not fully exploited until 1954 when the first silicon photovoltaic cell was developed by Daryl Chapin, Calvin Fuller and Gerald Pearson at Bell Laboratories in Berkley Heights, NJ, for the conversion of sunlight into electricity.

Power over fibre has been considered since the first production of fibre optic cables; however it has only recently become a viable power solution as the technology has improved. There are three components that make up an optically powered system; the source, the fibre and the power converter. The cost of producing high powered laser light sources has decreased and there is now a large variety of wavelengths available. The cost of fibres has also reduced, although the intention may be to power devices using existing fibre optic networks eliminating the cost of the fibre

completely. Furthermore, the increase in the efficiencies of PPCs has made power over fibre a cost effective and practical solution for a variety of applications.

1.3. Aims

The purpose of this project is to explore, via computer simulation and experimental validation, the properties of silicon and germanium photodiodes for low power harvesting applications, achieving the maximum possible output power generation from an optical fibre channelled laser light source. Moreover, to show that it is possible to launch a power signal and other signals through the same optical fibre and separate them without loss of information or power.

1.4. Significance

Communication over fibre optic cables has become very common since it was first developed in the 1970s. The idea of transferring power over the same cables has been around almost as long, although the technology required to produce low cost, high energy light sources is only now becoming available to warrant further research. Moreover, recent developments in photovoltaic cells mean power conversion efficiencies are now high enough that the total output power is now commercially useful.

Transmission of power over optical cables has many benefits as opposed to traditional electrical power techniques and can be used for a variety of applications. The insulating properties of glass and plastic fibres are particularly advantageous in high voltage and strong electromagnetic environments. The absence of an electric current also removes many of the problems associated in these situations [2]. Furthermore, the risk of sparks causing an explosion in gaseous environments is eliminated. In fibre optic communication networks, the cost of powering remote devices can be reduced as the power can be sent over the existing fibres.

1.5. Status

A number of papers have been written on the power harvesting properties of materials such as GaAs and InGaAs, as they are direct band gap materials and therefore efficient absorbers of light [3]. JDS Uniphase Corporation is the only

company in the world that produces these types of photovoltaic power converters. At present, I believe this to be the first study to consider silicon for this application. Although silicon is an indirect band gap material, and is therefore a poor absorber of light, in recent years there have been considerable advances in both photodiode and photovoltaic silicon technology to warrant this research. Moreover, previous work by Green, Zhao, Wang, & Wenham [4] shows that silicon has a high power conversion efficiency under illumination of monochromatic light.

1.6. Problems

Whilst the concept of photonic power has many advantages there are a few problems associated with optical power generation. Some lasers can produce extremely high powered light sources; optical fibres can only withstand certain levels of power before being damaged. High energy light sources may also cause the detector to heat up causing many negative effects such as reduced power conversion and physical damage. Furthermore, attenuation can increase dramatically at certain wavelengths; therefore the length of the optical cable may be relevant depending on the wavelength desired.

1.7. Objectives

1.7.1. Primary objectives

- To simulate the output power of a silicon photovoltaic cell, illuminated by a light source with a wavelength of 850nm and 980nm.
- To investigate how changing the properties of a silicon photovoltaic cell affects the current, and thus the output power of the cell and determine the most significant factors that affect power conversion efficiency.
- To experimentally prove a communication, sensing and power signal can be launched into one optical fibre and be separated without loss of information or power.

1.7.2. Secondary objectives

- To simulate the output power of a germanium photovoltaic cell, illuminated by a light source with a wavelength of 1310nm and 1550nm.

- To experimentally confirm some of the important results produced from the simulation package.
- To analyse experimentally, the effect of optical coupling mismatch between the optical fibre and the photovoltaic cell by varying the distance from the optical fibre to the cell.

1.8. Research Questions

1. Under illumination of near infrared laser light, what mechanisms limit the maximum output power of a standard silicon photovoltaic cell?
2. How do the physical dimensions of the photovoltaic micro-cell affect the output power?
3. Is one large device more efficient than an array of smaller devices, completely illuminated by a single light source?
4. What wavelength produces the maximum output power and why?
5. How does a germanium photovoltaic device compare to a silicon device with respect to output power generation?
6. What are the advantages of optical power generation rather than electrical power generation?
7. What limitations arise from the software used and what assumptions are made?
8. What applications could this device design be used for?

1.9. References

[1] National Research Council, "*Harnessing light: optical science and engineering for the 21st century*," National Academy Press, 1998, pp. 5.

[2] J.G. Werthen, "Powering Next Generation Networks by Laser Light over Fiber," *Optical Fiber Communication Conference and Exposition and The National Fiber Optic Engineers Conference*, February 2008.

[3] S.J. Wojtczuk, "Long Wavelength Laser Power Converters for Optical Fibers," *Photovoltaic Specialists Conference*, pp. 971-974, September 1997.

[4] M.A. Green, J. Zhao, A.Wang, and S. R. Wenham, "45% Efficient Silicon Photovoltaic Cell Under Monochromatic Light," IEEE Electron Devices Letters, vol. 13, no. 6, pp 317–318, 1992.

CHAPTER 2

THEORY

This chapter outlines the basic theory of photovoltaics with an emphasis on carrier transport mechanisms and recombination processes, which are key factors in determining the efficiency of a device. A basic understanding of the theory of states of matter in relation to conduction of electrically charged carriers is assumed.

2.1. Principle of Photovoltaics

The principle of photovoltaics is the generation of power from electromagnetic radiation, light. Since the 1950's, there has been a great deal of research into photovoltaics with a large amount of success. Nowadays the understanding of semiconductor physics is extensive with a huge variety of applications. The theory of photovoltaics suggests the efficiencies of photovoltaic cells should be relatively high. However, in practice the maximum obtainable efficiencies are considerably less than the theoretical limit [1]. The present challenge is to obtain efficiencies close to this limit.

2.2. The PN Junction

A photodiode is simply a PN junction with no external voltage applied. The N side of the junction has an excess of negatively charged electrons and the P side has an excess of electron vacancies. These vacancies behave like positively charged particles called holes [2]. This distribution causes a small potential difference which induces a small current flow as shown in figure 2.1.1. If the depletion region is illuminated by light, the photons can be absorbed by the charged particles giving them enough energy to break the bonds within their atoms and jump up into the conduction band and contribute to current flow, as shown in figure 2.1.4. This is the basic operation of all solar cells consisting of PN junctions engineered specifically to produce maximum power output.

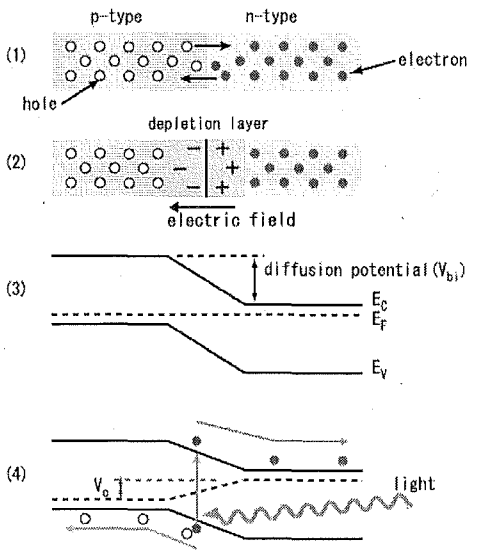

Figure 2.1. A PN junction (1) showing the depletion region and electric field (2). An energy band diagram (3) and the effect of a photon being absorbed (4), [3].

2.3. Carrier Generation

When a photon is absorbed it creates an electron-hole pair. For the pair to contribute to current flow, they must gain enough energy to break free of their atoms. This energy is defined as the band gap energy, E_g. A photon absorbed with less than the band gap energy will simply transfer its energy as heat and not increase the current flow. A photon with energy greater than the band gap will increase the current flow, with the production of an electron-hole pair, although any excess energy above the energy gap will be lost as heat or in the form of phonons. The energy of a photon is given by,

$$E = \frac{hc}{\lambda} \tag{2.1}$$

where, h is Planck's constant, c is the velocity of light and λ is the wavelength of the light. Therefore, for optimum efficiency, the photons of light illuminating the PN junction should have energies equal to the band gap energy, E_g, and hence a wavelength given by,

$$\lambda = \frac{hc}{E_g} \tag{2.2}$$

2.4. Band Structures

The band structure of a material will affect its optical and electrical properties. Figure 2.2 shows the energy band structure for silicon and gallium-arsenide. Silicon is an indirect band gap material. This means the transition of a carrier from one band to another cannot occur simply from the absorption of a photon only; the carrier must also undergo a change in momentum by absorbing a phonon. The energy band structure for GaAs shows clearly it is a direct band gap material and shows the upper and lower valleys in the conduction band [4].

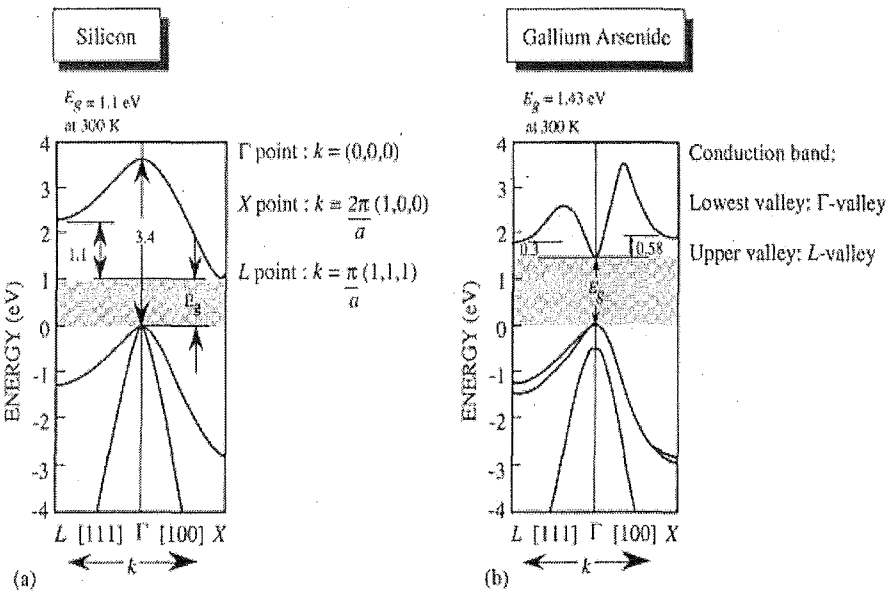

Figure 2.2. The band structure of (a) silicon and (b) gallium-arsenide [5].

2.5. Effective Mass

Electrons in the conduction band behave as if they are free from the Coulomb attraction of ions within the material and experience a force proportional to the applied electric field; $\underline{\mathbf{F}} = q\xi = m_0\underline{\mathbf{a}}$ which is related to its rest mass, m_0, and the acceleration vector, $\underline{\mathbf{a}}$. However, this does not take into account the interactions with the three dimensional lattice. To do this, the rest mass, m_0 is replaced by m*, the effective mass, which is derived from quantum theory. Essentially, an electron that interacts more with the lattice will have a higher effective mass and therefore lower drift velocity, than an electron that only interacts weakly with the lattice.

2.6. Carrier Transport Mechanisms

There are two transport mechanisms for charged carriers within a semiconductor: drift and diffusion.

2.6.1. Drift

Drift is the movement of a charged carrier as a result of an electric field. As mentioned above, the carrier experiences a force proportional to the electric field, defined by $\underline{\mathbf{F}} = q\xi$, where q is the charge of the carrier and ξ is the electric field. The momentum of the carriers is approximately given by,

$$\frac{1}{2}mv^2 \approx \frac{3}{2}kT \tag{2.3}$$

where, m and v are the carrier mass and velocity, respectively, k is Boltzmann's constant and T is the temperature. Therefore, the individual carriers have velocities equal to the saturation velocity given by,

$$v_{sat} = \sqrt{\frac{3kT}{m^*}} \tag{2.4}$$

where, m^* is the effective mass of the carrier. However, they collide with particles within the material causing a resistance, resulting in an average drift velocity, v_d, which is defined as the average displacement with respect to time, $v_d = \frac{\Delta x}{\Delta t}$, as shown in Figure 2.3.

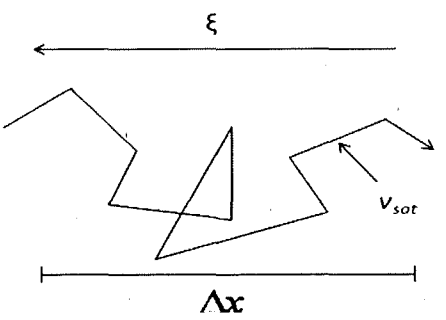

Figure 2.3. Electron drift.

The drift velocity is given by; $v_d = \mu\xi$ where μ is the mobility defined by $\mu = \frac{q\tau_d}{m^*}$, q is the charge of the carrier, t_d is the mean time between collisions, and m^* is the effective mass. This shows that the drift velocity is inversely proportional to the effective mass.

2.6.2. Diffusion

Charged carriers in the absence of an electric field will move around randomly due to thermal energy, colliding with each other. This random motion causes the carriers to distribute across the area of a device until there is equilibrium in concentration. Diffusion is the movement of charged carriers from a region of high concentration to a region of low concentration, due to Brownian motion as defined by Einstein.

2.7. Carrier Drift Velocity

The carrier drift velocity as defined above is determined by the carrier mobility and the applied electric field. GaAs has a high carrier drift velocity because it is a direct band gap material, which means it has minimal lattice or phonon scattering, and therefore, the electrons have a low effective mass of $0.067m_0$, resulting in high mobility. The drift velocity increases with an applied electric field. However, at a certain electric field potential the drift velocity decreases. This is because electrons gain enough energy to fall into the upper valley as shown in figure 2.2, where the density of states effective mass increases to $0.55m_0$, which results in lower mobility [4]. Silicon carriers have a lower drift velocity except in high electric fields, than GaAs, as shown in figure 2.4. The distance a generated carrier travels before recombining is called the diffusion length, L, and is given by,

$$L = \sqrt{D\tau} \tag{2.5}$$

where, D is the diffusion coefficient and τ is carrier lifetime. The longer the diffusion length, and hence the carrier lifetime, the more likely the carrier will contribute to generated current.

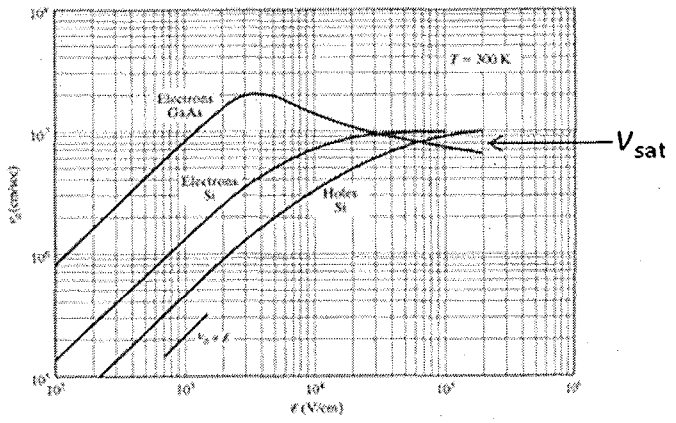

Figure 2.4. Carrier drift velocity as a function of electric field for Si and GaAs [4].

2.8. Absorption Coefficient

Another important factor when determining the appropriate material for a photovoltaic device is the absorption coefficient, α, defined as the relative number of photons absorbed per unit distance, in units of cm^{-1}, for a specific material. The absorption coefficient is related to the incident photon energy by,

$$I_v(x) = I_{v0}e^{-\alpha x} \tag{2.6}$$

where, $I_v(x)$ and I_{v0} are the intensity of photon flux at position x and the initial intensity at position 0, respectively. Therefore, the photon flux decreases exponentially with distance through the semiconductor material. If the absorption coefficient is large, photons are absorbed over a relatively short distance [4]. Figure 2.5 shows the absorption coefficient for various semiconductor materials. The span of the curves corresponds to the operating range of the materials.

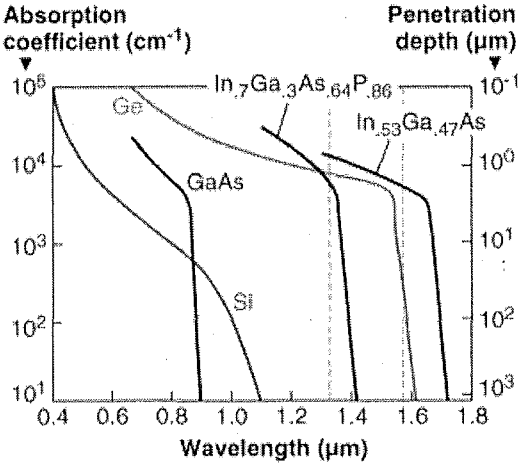

Figure 2.5. Absorption coefficient for various semiconductors showing penetration depth [6].

Using Figure 2.5, the appropriate depth of a device can be calculated for a required absorption percentage.

2.9. Doping

Intrinsic semiconductors are pure materials with a perfect lattice configuration. The electrical properties of an intrinsic semiconductor are determined by the structure of the lattice. Semiconductors that have impurities within their lattice are known as extrinsic semiconductors. Impurities within a crystal lattice can have a dramatic effect on its electrical properties [4].

The addition of a group 5 element into a silicon lattice (group 4) creates a spare electron as only 4 electrons are required for covalent bonding. The extra electron is only weakly bound to its atom and can easily jump up to the conduction band. This type of atom is called a donor impurity atom, which creates an electron energy state just below the conduction band without creating a hole energy state just above the valence band [4].

The addition of a group 3 element to a silicon lattice leaves a vacant hole as there are only 3 electrons available for bonding. As electrons within the lattice fall into the hole, the hole appears to move through the crystal lattice when an external field is applied. The hole contributes to current flow in the direction of the electric field. This type of atom is called an acceptor impurity atom, which creates a hole energy state just above the valence band without creating an electron energy state just below the conduction band [4].

Because doping a semiconductor changes the energy required for carriers to conduct, the doping concentrations within a device can dominate its electrical properties [7].

2.10. Recombination Processes

There are three recombination processes that occur within a photovoltaic device that contribute to the recombination rate, as shown in Figure 2.6.

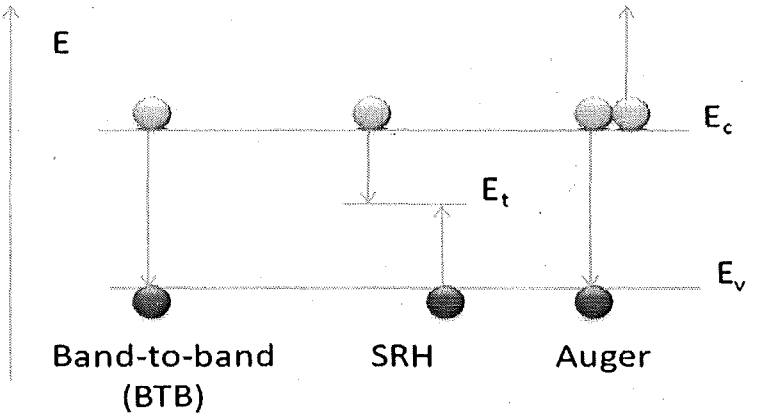

Figure 2.6. Semiconductor recombination mechanisms.

2.10.1. Band to Band Recombination

Band to band recombination is the process of an electron giving up its energy and falling from the conduction band to the valence band where it annihilates with a hole. This is typically a radiative transition in direct band gap material and depends on the density of available electrons in the conduction band and holes in the valence band [8]. Radiative recombination is basically the production of a photon similar to the incident photon.

2.10.2. Shockley-Read-Hall (S.R.H) Recombination

SRH recombination is due to impurities in the lattice of a semiconductor, energy is exchanged from photons to phonons, lattice vibrations. This creates energy levels within the band gap which act as traps, meaning it is easier for carriers to recombine, which in turn increases the recombination rate [4]. The net recombination rate for SRH in the simulation package [9], is given by

$$R^{SRH} = \frac{np - n_i^2}{\tau_p(n + n_1) + \tau_n(p + p_1)} \tag{2.7}$$

where n and p are the concentrations of electrons and holes, respectively, n_i is the intrinsic carrier concentration, τ_n *and* τ_p are the minority carrier lifetimes of electrons and holes respectively. The parameters n_1 and p_1 are the electron and hole concentrations if the Fermi level were at the energy level of the recombination centre (defined in the simulation manual).

2.10.3. Auger Recombination.

Auger recombination is a two stage process that involves three particles. It is a non-radiative transition where the energy is lost to the creation of a second electron-hole pair [7]. This process becomes more dominant when a device is highly doped and is thus a function of the carrier densities. It also dominates in II-VI materials such as HgCdTe [10].

2.11. Recombination Rate

The recombination rate is a result of the combination of all of the recombination processes mentioned above. It is directly proportional to the excess carrier concentration and is inversely proportional to the minority carrier lifetime.

2.12. Ideal Diode

The current produced by a photovoltaic cell can be approximated by the current generated from an ideal diode. The ideal diode equation is given by,

$$I_{total} = I_s\left(e^{qV/nkT} - 1\right) - I_{ph} \tag{2.8}$$

where, I_s is the reverse saturation current which is proportional to the dark current, I_{dark}, and I_{ph} is the photocurrent. Therefore,

$$I_{total} = I_{dark} - I_{ph} \tag{2.9}$$

2.12.1. Dark Current

The dark current, or reverse current of a photovoltaic cell, exists when there is a load present. The load causes a potential difference between the terminals which induces a current flow. This current flow is in the opposite direction to the photo-generated current, and therefore hinders the performance of a photovoltaic cell.

2.12.2. Photocurrent current

The photocurrent is proportional to the generation rate and therefore the incident optical power [7]. The maximum power produced is the point on the I-V

curve where the current multiplied by the voltage is at a maximum and is equated by setting the derivative of the power with respect to the voltage to zero. The illumination of a photovoltaic cell drives the I-V curve down as shown in figure 2.7.

2.13. Photovoltaic Cell Characteristics

There are a number of important parameters to consider when analysing the current-voltage characteristics of a photovoltaic cell. The parameters that define the performance of a solar cell are the short circuit current, I_{SC}, the open-circuit voltage, V_{OC}, the fill factor, FF, and the quantum efficiency, η. Figure 2.7 is a standard I-V curve for a photovoltaic cell showing some of these parameters.

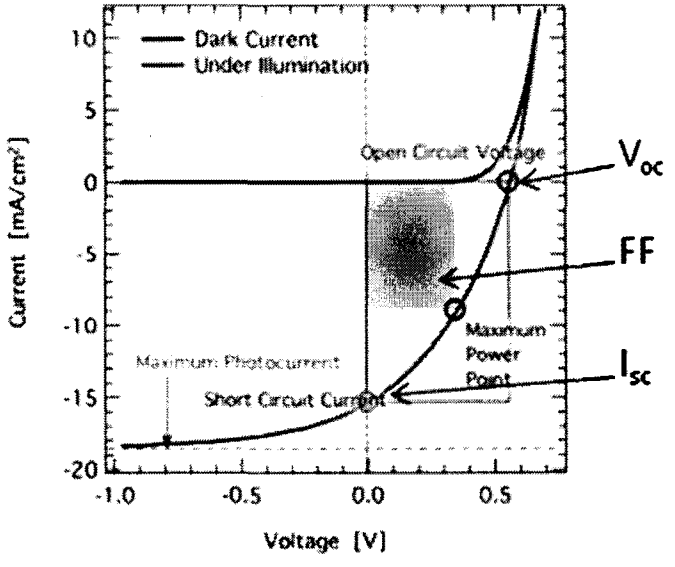

Figure 2.7. I-V curve of a photovoltaic cell under illumination [11].

2.13.1. Short circuit current

The short circuit current, as shown in figure 2.7, occurs when the load, and therefore the voltage, equals zero and is equivalent to the photocurrent [4].

2.13.2. Open circuit voltage

The open circuit voltage occurs when the resistive load is considered infinite, producing no net current, as shown in figure 2.7 [4].

2.13.3. Fill factor

The fill factor is the ratio of the maximum output power to the product of I_{SC} and V_{OC} [4]. The amount of area filled in figure 2.7 is given by,

$$FF = \frac{P_{\max}}{I_{sc}V_{oc}} \tag{2.10}$$

2.13.4. Quantum efficiency

The quantum efficiency, η, of a device is the ratio of the number of charged carriers collected to the number of photons incident on a device. The quantum efficiency for an incident wavelength, λ, radiant intensity, P_{opt}, and total current, I_λ, [12], is given by,

$$\eta = \frac{hcI_\lambda}{\lambda q P_{opt}} \tag{2.11}$$

2.14. Surface Reflectance

Surface reflectance is another important factor that limits the performance of a photovoltaic cell. The surface reflectance of a device depends on the refractive index of the material and its surroundings and is given by,

$$R = \left(\frac{n_2 - n_1}{n_2 + n_1}\right)^2 \tag{2.12}$$

where, n_2 is the refractive index of the material and n_1 is the refractive index of the surrounding medium, usually air, which has a refractive index of 1.

Under solar illumination, a bare silicon wafer can reflect as much as 30 percent of this incident light. This is why anti-reflective coatings (ARCs) are so important. The presence of a silicon dioxide layer can reduce the reflectance to about 10 percent, although more complex coatings made of TiO_2 or AlO_3, for example, can reduce the reflectance to less than 3 percent [13]. Under illumination of monochromatic light, specific coatings used to match the incoming wavelength can be used to minimise reflectance.

2.15. Optical Fibres

The theory of optical fibres gives an analysis of the properties of a light source leaving an optical fibre and determines the amount of coupling that occurs between the fibre and the detector. Figure 2.7 shows the Gaussian profile of a laser.

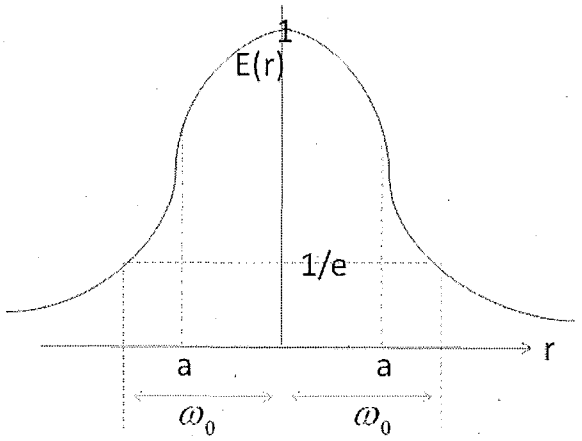

Figure 2.8. Gaussian representation of field distribution.

ω_0 is the field spot size; at this radial position the light field intensity drops to 37% of its maximum. To obtain a value for the spot size, the numerical aperture, NA, must be calculated from

$$NA = \sqrt{n_1^{\,2} + n_2^{\,2}} \tag{2.13}$$

where, n_1 and n_2 are the refractive indices of the core and the cladding, respectively. Equation (2.14) is then used to calculate the normalised frequency, V from

$$V = \frac{2\pi a}{\lambda} NA \tag{2.14}$$

where a is the beam width radius, and λ is the wavelength of the light. The result can then be used to calculate the spot size, ω_0, which effectively determines the amount of coupling between the fibre and the detector [14];

$$\omega_0 = a\left(0.65 + \frac{1.619}{V^{3/2}} + \frac{2.879}{V^6}\right) \tag{2.15}$$

2.16. References

[1] M. A. Green "Third Generation Photovoltaics: Ultra-High Conversion Efficiency at Low Cost," Progress in Photovoltaics: Research and Applications, Vol 9, Issue 2, pp 123-135, 2000, Wiley.

[2] S. Wenham, M. A. Green, M. Watt, & R. Corkish, *Applied Photovoltaics*, 2nd edition. Earthscan, 2007.

[3] Pn Junction diagram, n.d. Retrieved May, 2010, from http://commons.wikimedia.org/wiki/File:PnJunction-PV-E.PNG

[4] D.A. Neaman, *Semiconductor Physics and Devices*, 3rd edition, McGraw-Hill, New York, New York, 2003, pp. 620-621.

[5] Semiconductors Optics and Optoelectronics, n.d. Retrieved May, 2010, from http://kottan-labs.bgsu.edu/teaching/workshop2001/chapter5.htm.

[6] M. Morse, "Semiconductor Detectors: Germanium on silicon approaches III-V semiconductors in performance" laser-focus-world, vol. 43 no. 5, May 2007.

[7] S.L. Chuang , *Physics of Optoelectronic Devices*, 1st edition, New York: Wiley, 1995, pp. 597–598.

[8] B. Van Zeghbrook, Principles of Semiconductor Devices, 2002. Retrieved April, 2010, from http://link.edu.ioffe.ru/pti80en/alfer_en

[9] SEMICAD DEVICE Version 1.2 manual, 1994. Dawn Technologies Inc Sunnyvale, CA, USA.

[10] Y. Jiang, M. Teich, W. Wang, J. Meyer, "Auger Recombination in HgCdTe Quantum Wires and Quantum Boxes," Journal of Applied Physics, Vol. 71, Issue 7, pp. 3394-3398, 1992.

[11] Deibel, Intermediate: Current-Voltage Characteristics of Organic Solar Cells. 20th May 2009. Retrieved from

http://blog.disorderedmatter.eu/2008/03/05/intermediate-current-voltage-characeristics-of-organic-solar-cells/

[12] S. Hinckley, P. Jansz, "Stacked Homojunction Effects on Crosstalk and Response Resolution in CMOS Compatible Photodiode Arrays," IFIP 10.5 Conference on Very Large Scale Integration System-on-Chip, 2005.

[13] G. Smestad, *Optoelectronics of Solar Cells, 1st edition*, SPIE,Washington 2002.

[14] P. L. Chu, *ELEC8350 Theory of Optical Fibres*, University of New South Wales, Sydney 2002.

CHAPTER 3

LITERATURE REVIEW

This chapter gives an overview of the sources of literature used, and a brief summary of relevant research literature. This includes a review of power over fibre, advantages and applications of fibre optic power systems, laser profiles and the physics of optical fibres, as well as different materials considered for use as photovoltaic power converters.

3.1. Significant Journals

A number of Journals are strongly related to the specific topic. These journals are available in full text, and will be used as primary reading sources. The primary journals include;

- Solar Energy Materials & Solar Cells, by the Solar Energy Research Institute.
- IEEE Transactions on Electron Devices.
- Journal of Semiconductors, by Institute of Physics, U.K.

3.2. Databases

A number of databases have been used in the sourcing of literature. These databases have contributed to improving the efficiency of sourcing relevant literature by relating similar articles. The most significant databases include;

- The International Society for Optical Engineering (SPIE) Digital Library.
- The Institute of Electrical and Electronic Engineers (IEEE) Xplore Digital Library.
- The Institute of Physics (IOP) Electronic Journals.

3.3. Authors and Research Groups

A number of key authors and research groups have been identified. One of the most significant authors in the field of silicon photovoltaics is Professor Martin A. Green of the University of New South Wales. Other noteworthy authors belong to research groups, including but are not limited to;

- Spire Corporation, Bedford, MA, USA.
- Division of Engineering, Brown University, RI, USA
- Photonic Power Business Unit, JDSU Corporation, CA, USA.

3.4. Literature Summary

This literature summary will look at the individual areas which contribute to the overall scope of the topic. These include the concept of power over fibre, the advantages and application of photonic power systems, the relevant properties of laser light and optical fibres. Relevant research into different materials such as silicon, gallium-arsenide, germanium and other heterostructures for use as photovoltaic power converters is also detailed. Finally, a review of previous design configurations is discussed.

3.4.1. Power over fibre

The concept of power over fibre implies that optical power is generated from an electrical source through the use of a laser diode, transferred through an optical fibre, and then converted back to electricity by a photovoltaic power converter (PPC), in order to power an electrical device.

3.4.2. Advantages and applications of fibre optic power systems

Fibre optic cables have many advantages over traditional copper wires mainly associated with their immunity to electromagnetic noise. Although the power transmission over optical fibres in far less efficient than copper wires, approximately 25 percent compared to almost 100 percent [1], supplying power over optical fibres is

advantageous in specific applications. Any high voltage environment poses a particular problem for electrically powered devices in measuring current [2]. Optically powered devices, because of their immunity to electromagnetic interference and lightning strikes, provide a much simpler and safer solution. Optically powered current transducers (OPCT) are lightweight and agile compared to large expensive transformers used to isolate sensors from ground potential [2].

Photonic power systems have no risk of causing a spark and explosion in gaseous environments. Silica fibres are also less chemically reactive in corrosive environments where copper cables could easily carode.

Optical power systems also have many medical applications, such as equipment used in magnetic resonance imaging (MRI), where high magnetic fields interfere with electrical systems causing many problems [3]. Optically powered devices may eliminate many problems associated with implanted medical devices, removing the need for batteries and therefore reducing energy restrictions. This opens the door for more complex high energy devices such as an implantable defibrillator or artificial implantable heart, which in the past were not possible due to the large batteries required [4]. Moreover, optical fibres are inert materials meaning they are biocompatible, reducing the risk of infection. Also, optical fibres can be extremely thin, comparable to the diameter of a human hair, this means "the end of a fibre close to the skin would be sealed by natural means (epithelialisation)" [4], an advantage already being exploited in other medical applications.

3.4.3. Laser profile

The light leaving an optical fibre has a Gaussian profile. In order to determine the most effective size of PPC to produce maximum power, the Gaussian beam should be analysed. The larger the area of the PPC, the greater the amount of light that is collected, however if the PPC is too large the voltage produced will start to drop off. Wojtczuk [1], showed that, in general, the radius of the PPC should be twice the 1/e beam width radius, agreeing with previous studies. The 1/e beam width radius is where the intensity of the light is approximately 37 percent of its maximum at the centre and is equivalent to the field spot size, ω_0, which can be calculated from the wavelength of the light and the refractive indices of the fibre optic cable. Hence, the

ideal width of the PPC can be calculated. It is worth noting that if the device is too small with respect to the beam width, the power conversion drops off rapidly, whereas a relatively large PPC with respect to the beam width only gradually reduces the efficiency.

3.4.4. Optical fibres

The attenuation of a signal in an optical fibre is very important as it determines the maximum distance between successive repeaters, which determines the overall cost of a fibre optic network. Figure 3.1 shows the attenuation in a silica fibre against wavelength.

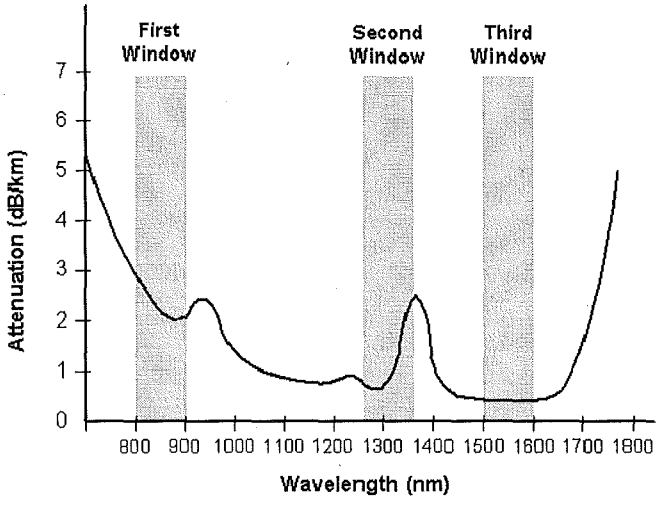

Figure 3.1: Attenuation in an optical fibre against wavelength showing the three optimum windows [5].

The attenuation in a silica fibre at 0.85um is approximately 3dB/km and is referred to as the first window. Repeaters must be spaced less than 100km apart. This was the wavelength used in the first generation of optical fibre communication networks and was the longest wavelength light source available until the 1980s. The second window is at a wavelength of 1.3um where the attenuation is 0.5dB/km. Modern communication systems aim to utilise the third window, 1.55um. The attenuation of 1.55um wavelength light is less than 0.2dB/km in standard silica fibres [6]. However, attenuation less than 0.01dB/km can theoretically be achieved with fluoride-glass fibres for wavelengths of 2um and above, as Rayleigh scattering decreases as $1/\lambda^4$ [1].

3.4.5. Silicon

Silicon photovoltaic cells have progressed steadily in complexity and performance over the last 25 years, predominantly due to extensive research by the University of New South Wales Photovoltaics Special Research Centre. Before 1983, the maximum reported efficiency of crystalline silicon was close to 17 percent [7]. The UNSW research team has since shown that the electrical activity at the surface of a cell could be reduced by introducing a thin layer of oxide along the top surface, subsequently improving its efficiency. Having already proved that low resistance substrates would improve efficiency, they then improved contact passivation by using MIS tunnelling contacts and increased the maximum efficiency from 17 percent to over 20 percent [8]. Another improvement resulting from modified device designs from the UNSW team was the development of the buried contact cell. The main advantage of this cell, whilst benefitting from the advances of previous designs, was that the metal contacts are formed only in heavily doped regions in the cell. This design was then commercialised by BP Solarex.

The motivation behind these improvements came from a need to increase the efficiency of a cell under solar irradiation. However, the improved surface properties and reduced area contacts to reduce recombination would obviously increase cell performance under monochromatic illumination, which is the main objective in this thesis.

Nevertheless almost all research on silicon-based photovoltaic cells is still based on its broadband spectral response. This is because the main goal for researchers is to improve the efficiency of converting sunlight into electricity, hence solving many of the modern concerns for the reduction of damage to the environment and energy sustainability for the future. In order to achieve this goal there are many different approaches being taken: advanced light trapping techniques, including the development of more advanced anti-reflective coatings and intricate surface geometries [7], complex light concentrating designs with lenses and mirrors for concentrations as high as a thousand suns [9]; and extensive research into silicon thin film technologies.

Moreover, there is so much diversity associated with the development of each step in the manufacturing process of solar cells, from growing crystals, laser scribing [10], diffusion and ion implantation methods and printing of thin films in a similar way to conventional laser printing [11], that only an entire PhD thesis would suffice in outlining the engineering advances achieved over recent years and the possible predictions for the future of the photovoltaic industry.

Many of the developments mentioned above are significant in increasing the efficiency of a photovoltaic device under illumination of monochromatic light. Research into the increased responsivity of silicon photovoltaic cells illuminated by solar radiation is improving their efficiency as stated in the ARC Photovoltaics Centre of Excellence 2008 Annual Report "We benefit greatly from this change because our cells push the boundaries of response far past the edges of the visible spectrum", [12]. The research is relevant to this paper as it is concerned with silicon's responsivity in the Infrared range.

Silicon responds to light within the 300nm to 1100nm range, peaking at around 850nm. It is an indirect band gap material, and therefore a relatively poor optical material. However, in recent years the efficiency of silicon solar cells has increased above 24 percent under solar illumination and above 45 percent under monochromatic light, using a passivated emitter, rear locally diffused cell (PERL cell), as shown in figure 3.2, which is designed specifically to trap as much of the incident light as possible, by effectively increasing the path length of the light by as much as 26 times [7].

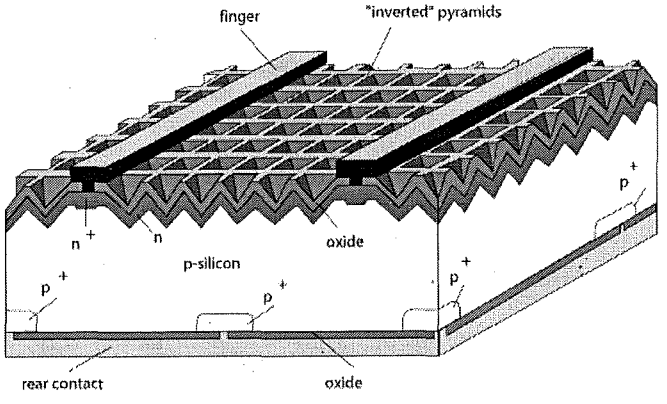

Figure 3.2: PERL cell (passivated emitter, rear locally diffused cell) [13].

Although long wavelength light is absorbed by silicon, it only interacts weakly. By reflecting the light within a device and trapping it, it is possible to increase its efficiency considerably, "close to 40% for light at 1.064 microns" [7].

In optimising the efficiency of a device, many parameters must be considered in order to reduce losses which are determined solely by the band gap, E_g, of the semiconductor. Some of the most important factors in the design of a photovoltaic device are: doping concentrations, thickness of the emitter and base, and contact structure. These factors have been shown to determine the level of resistance within each area of the device and therefore determine the collection probability and its efficiency [14]. Figure 3.3 shows a standard silicon photovoltaic micro-cell.

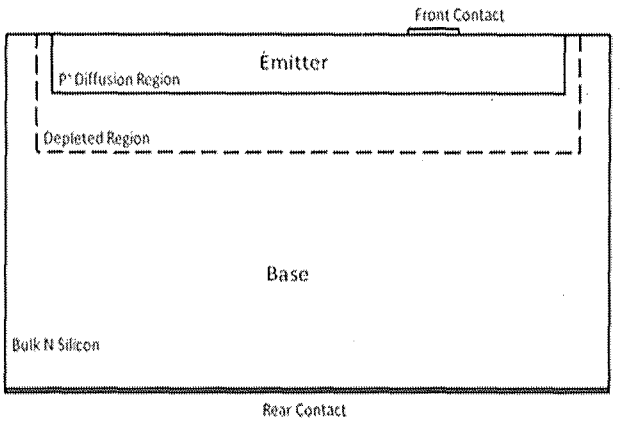

Figure 3.3: Standard silicon photovoltaic microcell.

Loss processes that occur within a photovoltaic device are directly associated with its efficiency. Hence, an understanding of these processes and how to reduce their effect is essential. In a standard model there are four loss processes, in which two are defined by junction and contact voltage loss. However, the two most dominant loss processes are thermalisation loss and recombination loss. Thermalisation loss is due to generated electron-hole pairs gaining more energy than the band gap energy which essentially is not required and is therefore lost as excess heat [15]. This loss is minimal in this application as the use of monochromatic light can provide a specific amount of energy that approximately matches the band gap energy. The most significant loss process associated with energy harvesting from a monochromatic source is therefore recombination. There are three types of recombination that occur, Shockley-Read-Hall recombination, Radiative recombination and Auger recombination. These recombination processes can be

decreased by modifying the device structure. Both Shockley-Read-Hall and Auger recombination affect the minority carrier lifetime by reducing it. At low doping concentrations, SRH recombination dominates whereas Auger recombination becomes increasingly more significant as the doping concentration increases [16].

In 1984 M. A. Green [17], was the first to give a modern analysis of silicon solar cells, defining optimum doping levels which were defined by the effect of Auger recombination, the most significant restriction on the performance of a silicon photovoltaic cell. Another dominant factor is surface recombination, which limits the performance of thin cells significantly. The effect of surface recombination is reduced by increasing the thickness of the cell. A 1um thick cell efficiency decreases from 24.7% to 19.8% when surface recombination is taken into account, whereas a 400um thick cell's efficiency reduces from 28.5% to 26.8% [8].

3.4.6. GaAs

GaAs has many advantages over silicon as it is direct band gap material with a large band gap energy. It is less sensitive to heat and generates less noise than silicon when operated at high frequencies. GaAs is also, unlike silicon, a good electrical substrate, it can provide isolation between devices due to its resistivity resulting from the large energy gap between bands. It has been used for a large array of optical applications as it is efficient in producing light as well as absorbing it [18]. GaAs has been a particularly favourable material for use as a photovoltaic power converter (PPC) because of its high quantum efficiency, 90%, and relatively high responsivity of approximately 60% at a wavelength of 0.82 microns [1]. In general, experimental evidence shows that the higher the band gap energy of a material, the higher the photovoltage and fill factor will be, as shown in table 3.1.

Table 3.1: Caparison of I-V Data of Single Junction PPCs.

Type	λ um	R at λ A/W (QE)	Test Jsc A/cm^2	Voc V	Fill %	Eff %
1.42eV GaAs	0.82	0.59 (90%)	0.81	1.1	88	57
0.74eV InGaAs	1.55	1.06 (85%)	5.1	0.48	67	34
0.55eV InGaAs	2.1	1.18 (70%)	3.2	0.29	63	22

Therefore, as GaAs is responsive to short wavelengths it produces a high open circuit voltage, 1.1V, and has a high fill factor of 88% at this wavelength [1]. It has a cutoff wavelength of 0.87 microns which agrees strongly with the statement made by Wojtczuk [1], "One would always like to select a LPC (Laser Power Converter) whose cutoff wavelength is just above the incident laser radiation". Moreover, a GaAs PPC would be transparent to any signals above 0.87 microns, making it a useful device in modern optical communication networks. Lasers producing light within GaAs optimum range, 790nm to 850nm, are readily available and can produce up to 5W of power [2].

3.4.7. Germanium

A comparison of a Germanium photovoltaic cell will be made with that of a Silicon photovoltaic cell. Germanium photovoltaic cells have a higher efficiency than silicon photovoltaic cells and are much lighter; however because of the high cost and brittle nature of the material, it is only used by NASA for solar cells on spacecraft. Engineers at the University of Utah, have devised a new way to slice thin wafers of the material, reducing the waste and hence the cost of production [19]. Although silicon is still far cheaper to produce, for specific applications, the benefit of high efficiency may outweigh the disadvantage of cost.

3.4.8. Heterostructures

Heterostructures are basically devices that contain one or more heterojunctions, i.e. there is a junction between two different materials. Historically most of the parameters of semiconductor devices were controlled by doping concentrations; the advantage of a heterojunction is that the energy gap between the conduction band and the valence band can be engineered quite specifically. Many other properties such as "effective masses and mobilities of charge carriers, refractive indices, electronic band structure," [20], can also be controlled with relative ease and increased accuracy.

Many different heterostructures have been designed, fabricated and analysed over the last thirty years for a variety of applications, most promisingly for laser diodes and PPCs. NG & Nakano [21], describes in detail the properties of a

GaInAsP/InP double hetero PPC with a large spectral response between 0.98um and 1.15um and hence optimised for power conversion at 1.06um. This type of heterostructure is effective as a PPC because it has relatively low surface recombination due to a wide band gap window on top of the active layer. Their results show that the quantum efficiency of a device is directly associated with minority carrier lifetimes and hence the electron and hole diffusion lengths, which in turn determine the amount of carriers which are collected. They report a quantum efficiency of 82 percent, a fill factor of 76 percent, and therefore a total power conversion efficiency of approximately 30 percent.

Heterostructures, as mentioned above, can be engineered to have a small band gap energy and thus respond to long wavelength laser light. The main advantage of this is that they operate at wavelengths which correspond to the attenuation minima of silica fibres, such as 1.31um and 1.55um. As stated earlier, silicon responds well to a wavelength of 0.85um which is also an attenuation minima, although it is not as significant as the longer wavelengths. If a PPC can respond effectively to a light source with a wavelength greater than 2.1um, then it could be used in free space, non-fibre applications as the laser light would be safe and cause no damage to the human eye. The disadvantage of using these heterotructures is that the low band gap energy results in a low open circuit voltage, meaning several devices need to be connected in series to obtain an array of sufficient voltage [22].

3.4.9. Design configurations

In order to boost the voltage output of a real PPC, a number of devices must be connected in series so that the voltage from each device combines. This can be achieved by monolithically integrating the separate junctions on one insulating wafer [1]. If the device is to be connected to a fibre optic cable, as in this case, the overall design of the PPC can be fabricated in a circular shape with each section looking like a slice of cake as shown in figure 3.4.

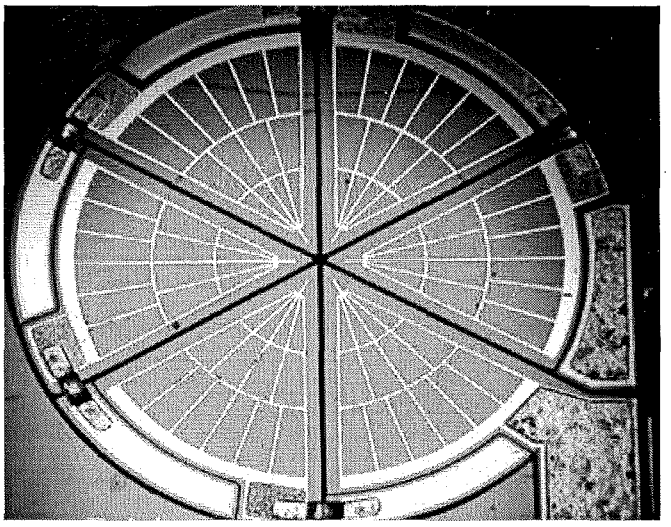

Figure 3.4: A photograph of photovoltaic power converter [2].

This orientation ensures the photocurrents produced in each of the series connected junctions will be similar. It is worth noting that each segment must be isolated electrically before being reconnected in series [2]. This design configuration has been considered for a long time, with the number of segments depending on the materials used and the required voltage. Ng and Nakano [21], describe a GaInAsP/InP circular PPC with 12 segments producing a total open circuit voltage of approximately 8V. Hwang, et al [23], suggest using a GaAs/AlGaAs PPC with 3 segments to produce over 3 volts. Werthen [2], shows a GaAs PPC with 6 segments producing just less than 6 volts for driving any 5 volt application.

Alternatively, an inexpensive DC-DC switching power converter chip may be used in conjunction with a single junction cell to increase the voltage. This has the benefit of the ability to provide a wide range of voltages as it can be programmed with external resistors. However, this is a larger solution, whereas a multijunction PPC is much more compact [1].

The total efficiency of a single junction PPC is slightly greater than a multijunction PPC, because there is more surface area being illuminated by light. In other words, the multijunction PPC has more dead photoarea. The relationship between single and multijunction PPCs is, in fact, a simple trade-off between current and voltage. The total voltage is the product of the number of junctions whereas the output current reduces by a factor corresponding to the number of junctions [1].

3.5. References

[1] S.J. Wojtczuk, "Long Wavelength Laser Power Converters for Optical Fibers," *Photovoltaic Specialists Conference*, pp. 971-974, September 1997.

[2] J.G. Werthen, "Powering Next Generation Networks by Laser Light over Fiber," *Optical Fiber Communication Conference and Exposition and The National Fiber Optic Engineers Conference*, February 2008.

[3] R. Gassert, D. Chapuis, H. Bleuler, & E. Burdet, Sensors for Applications in Magnetic Resonance Environments. Mechatronics, IEEE/ASME Transactions on Electron Devices. Vol. 13, pp.334-335, 2008.

[4] C. Valle, L. Munoz, "Photovoltaic Energy Supply System with Optical Fibre for Implantable Medical Devices", 1998.

[5] The Attenuation-Wavelength Curve and the Transmission Windows of an Optical Fiber, 2010. Retrieved June, 2010, from http://macao.communications.museum/eng/exhibition/secondfloor/moreinfo/2_8_3_OpticalFibres.html.

[6] P. L. Chu, *ELEC8350 Theory of Optical Fibres*, University of New South Wales, Sydney 2002.

[7] M.A. Green, J. Zhao, A.Wang, and S. R. Wenham, "45% Efficient Silicon Photovoltaic Cell Under Monochromatic Light," IEEE Electron Devices Letters, vol. 13, no. 6, pp 317–318, 1992.

[8] M.A. Green, J. Zhao, A.Wang, and S. R. Wenham, "Very High Efficiency Silicon Solar Cells- Science and Technology," IEEE Transaction on Electron Devices, Vol. 46, No. 10, pp 1940-1947, 1999.

[9] J. Gordon, E. Katz, D. Feuermann, & M. Huleihil, "Toward Ultrahigh-Flux Photovoltaic Concentration," Applied Physics Letters, Vol. 84, No. 18, 2004.

[10] F. Coville, "Ultrafast Laser-Based Tools Enhance Solar Cell Efficiencies," in *Proceedings of SPIE Frontiers in Ultrafast Optics: Biomedical, Scientific, and Industrial Applications X*, pp. 758913-1–758913-9, 2010.

[11] Wong, Ready, Lu, & Street, "Hydrogenated Amorphous Silicon Thin Film Transistor Arrays Fabricated by Digital Lithography," IEEE electron Device Letters, Vol. 24, No. 9, pp. 577-579, 2003.

[12] A. Ho-Baille, ARC Photovoltaics Centre of Excellence 2008 Annual Report, pp 6, 2008.

[13] PERL cell, 2009. Retrieved June, 2010, from http://www.kanoda.com/PVTechnologyandIndustry.html

[14] P. Kittidachachaun, T. Markvart, D. Bagnall, "Optimisation, design and fabrication of high efficiency p-n junction solar cell," The University of Southampton, 2003.

[15] M. A. Green, "Third Generation Photovoltaics: Ultra-High Conversion Efficiency at Low Cost," Progress in Photovoltaics: Research and Applications, Vol 9, Issue 2, pp 123-135, Wiley, 2000.

[16] H. Lanyon, "The Physics of Heavily Doped N+ P Junction Solar Cells," Solar Cells, Vol. 3, No. 4, pp. 289-311, 1981.

[17] M. A. Green, "Limits on the Open Circuit Voltage and Efficiency of Silicon Solar Cells Imposed by Intrinsic Auger Processes", IEEE Transaction on Electron Devices, Vol. ED-31, pp. 671-678, 1984.

[18] D.A. Neaman, *Semiconductor Physics and Devices*, 3rd edition, McGraw-Hill, New York, New York, 2003, pp. 620-621.

[19] Bamberg, Rakwal, Thin Germanium Wafers Shine Bright for Solar Cell Efficiency, 28th September 2008, Retrieved from http://www.scientificblogging.com/news_releases/thin_germanium_wafers_shine_bright_for_solar_cell_efficiency

[20] Zh. Alferov, V. Andreev, & N. Ledentsov, Semiconductor Heterostructures, n.d. Retrieved May, 2010, from http://link.edu.ioffe.ru/pti80en/alfer_en

[21] W. NG, K. Nakano, "A Monolithic GaInAsP/InP Photovoltaic Power Converter," IEEE Transaction on Electron Devices, Vol. ED-29, No. 9, pp 1449-1454, 1982.

[22] Giles, Dentai, Burrus, Kohutich, Centanni, "Microwatt- Power InGaAs Photogenerator for Lightwave Networks," IEEE Photonics Technology Letters, Vol. 9, No. 5, pp. 666-668, 1997.

[23] N. Hwang, Y. Song, T. Atay, & A. Nurmikiko, "Photovoltaic Energy Converter as a Chipscale High Efficiency Power Source for Implanted Active Microelectronic Devices," Proceedings of the 26th Annual International Conference of the IEEE EMBS, 2004.

CHAPTER 4

SIMULATION RESEARCH PAPERS

This chapter includes three papers containing results of various simulations of photovoltaic cells that have been submitted, peer reviewed and accepted to different conferences within Australia. Each paper has been published in the relevant conference proceedings.

4.1. Photovoltaic Micro-Cell Design for Distributed Power in Sensor Networks

G. Allwood, G. Wild and S. Hinckley, Proceedings of the 2010 Conference on Optoelectronic and Microelectronic Materials and Devices (COMMAD).

4.1.1. Abstract

We present a new study of power over optical fiber, for use in optical fiber smart sensor networks, using silicon-based photovoltaic micro-cells. A number of parameters in the design of the micro-cell for implementation in a power converter chip have been investigated. Matching the beam profile to the active region, as well as maximizing the contact area improves the device efficiency. The effect of doping profile and junction type on the device performance, suggests silicon is a cost effective and suitable material for this application.

4.1.2. Introduction

Research on III-V material photovoltaic power converters, (PPC's) usually complex heterostructures involving GaAs or InP, has shown optical power conversion as high as 50% [1]. Terrestrial solar cell development for high power applications using silicon-based cells has also indicated high efficiencies for these types of solar cell structures for monochromatic illumination [2]. Here, we suggest a novel idea of coupling a silicon photovoltaic micro-cell to an optical fiber for use as a PPC. Silicon, although not the most efficient optical power converter, is suitable for this application

because of its high responsivity between 600nm and 900nm, as well as its obvious low cost of fabrication.

In this paper, we present the results of a study to optimize the power output of a silicon-based pn junction photovoltaic micro-cell for monochromatic optical fiber illumination. The effect of a number of device structure and material parameters have been simulated and optimized, so that a dedicated PPC chip can be used to meet the power budget of a distributed optical fibre smart sensor system currently being developed. All of the results were obtained using an incident optical power of 100mW, so that the output power equates to efficiency.

4.1.3. Results

Fig. 4.1.1 shows a graph of device thickness against incident wavelength and the corresponding maximum efficiency.

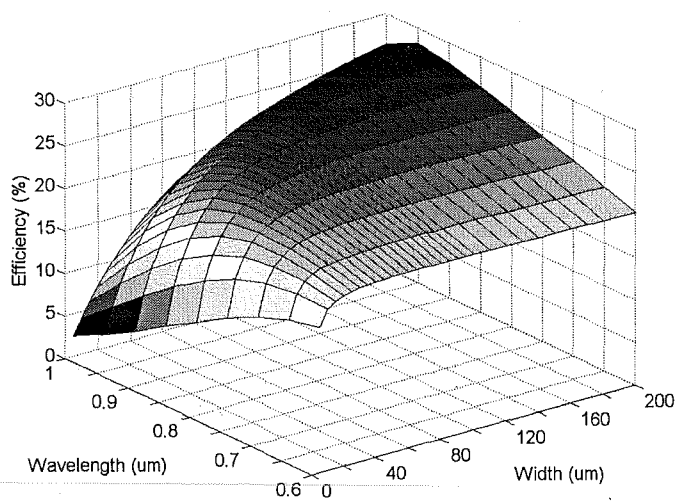

Fig. 4.1.1: Maximum efficiency for device thickness against wavelength.

Fig. 4.1.2 shows a logarithmic graph of wavelength against thickness. The equation can be used to predict the optimum thickness for a given wavelength, i.e. the optimum thickness for a wavelength of 980nm is approximately 265um.

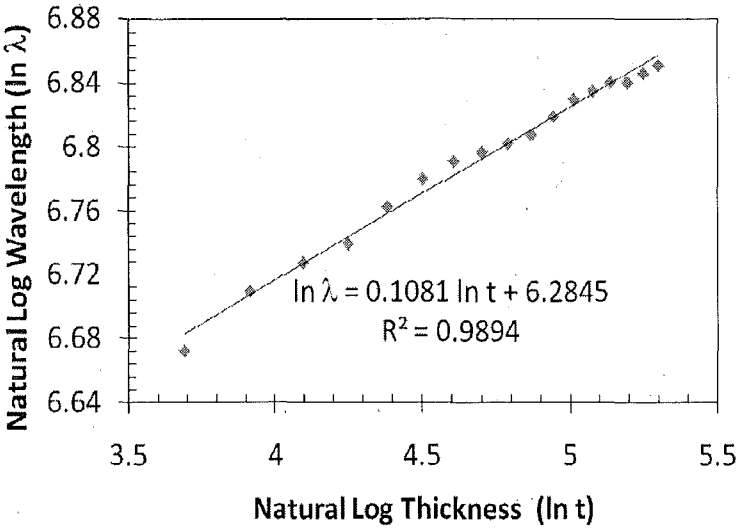

Fig. 4.1.2: Logarithmic graph of wavelength against thickness.

Shown in Fig. 4.1.3 is the relationship between wavelength and output power for various beam widths. The optimum beam width occurs at 300um, the same width of the emitter region.

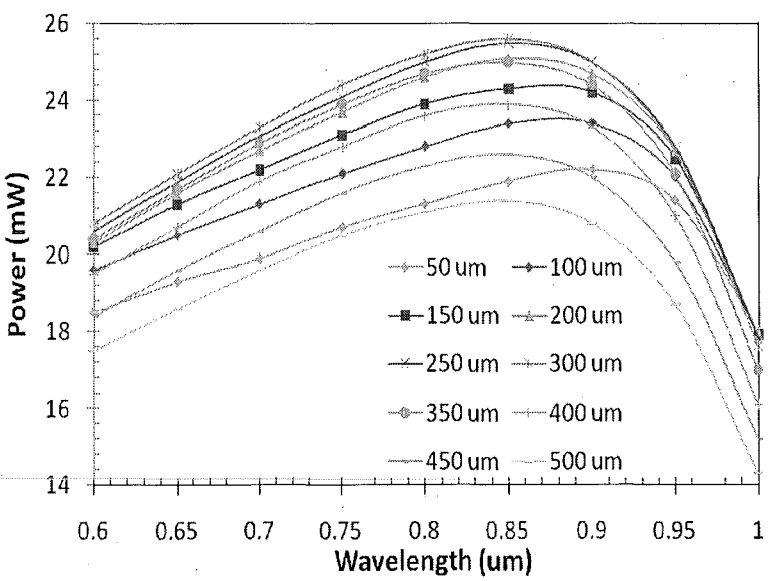

Fig. 4.1.3: Maximum output power against wavelength for various beam widths.

Fig. 4.1.4 and Fig. 4.1.5 show the effect of both the emitter and base doping concentrations on output power for a p+n device and a n+p device, respectively.

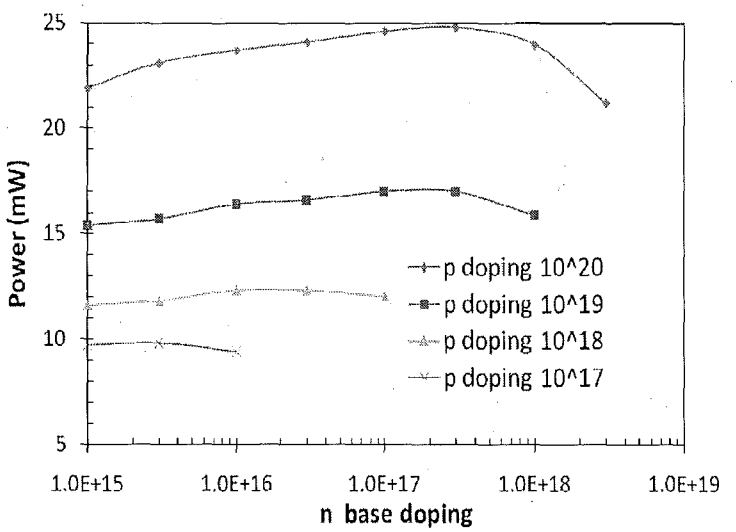

Fig. 4.1.4: Maximum power against n doping concentration for various p doping concentrations in a p+ n device.

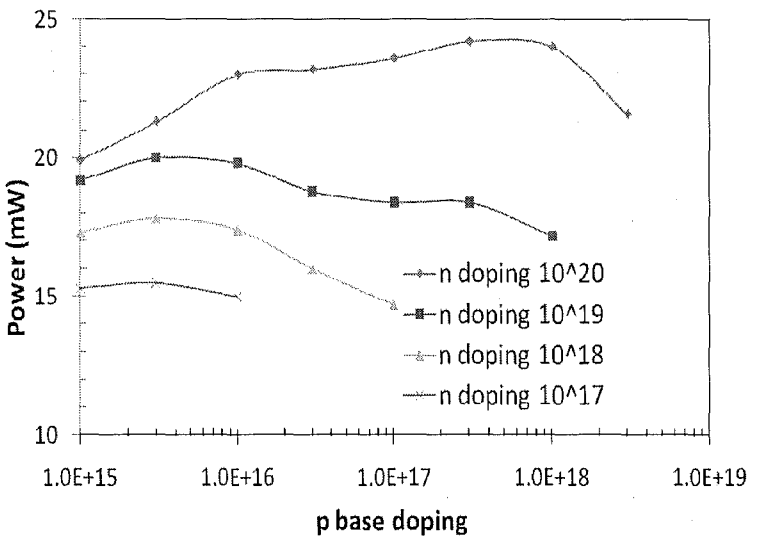

Fig. 4.1.5: Maximum power against n doping concentration for various p doping concentrations in an n+ p device.

The n+p device performs better at lower emitter doping concentrations because the mobility of the minority carriers, electrons, is higher than that of the p+n minority carriers, holes.

A consideration was made to increase the size of the anode so that it was the same width as the emitter region. This improved the collection of carriers considerably and therefore improved the efficiency. Finally, using the results from all of the previous considerations, the I-V characteristic of the most theoretically efficient PPC, producing the maximum output power, was simulated. Table 4.1.1 shows the

parameters used in this simulation, and the corresponding output characteristics. The corresponding I-V curve and power curve are shown in Fig. 4.1.6.

Table 4.1.1: Device parameters.

Parameter	Value	Units
Beam width	300	um
Wavelength	850	nm
Base n-doping	$3x10^{17}$	cm^{-3}
Emitter p-doping	$1x10^{20}$	cm^{-3}
Short circuit current	62.5	mA
Open circuit voltage	0.78	V
Fill factor	81.2	%
Output Power	39.6	mW

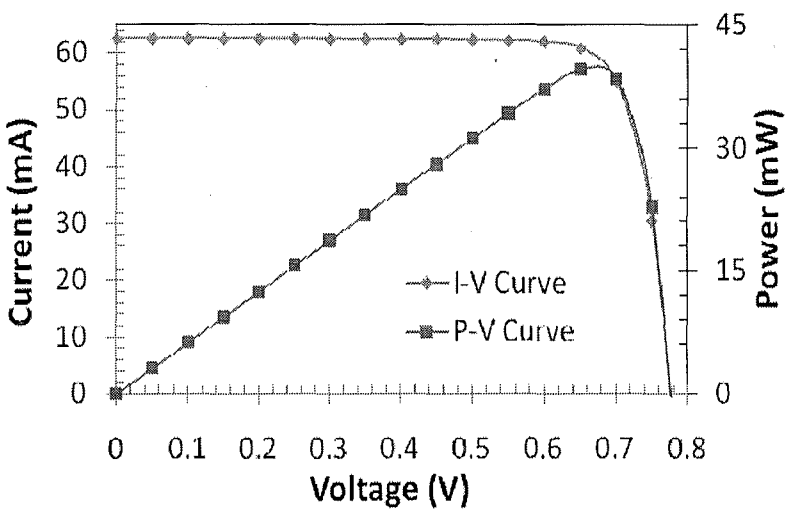

Fig. 4.1.6: I-V curve and power curve for the optimum designed silicon PPC.

4.1.4. References

[1] J.G. Werthen, "Powering Next Generation Networks by Laser Light over Fiber," Optical Fiber Communication Conference and Exposition and The National Fiber Optic Engineers Conference, February 2008.

[2] M.A. Green, J. Zhao, A.Wang, and S. R. Wenham, "45% Efficient Silicon Photovoltaic Cell Under Monochromatic Light," IEEE Electron Devices Letters, vol. 13, no. 6, pp 317–318, 1992.

4.2. Photovoltaic Micro-Cell Design for Distributed Power-over-Fibre Optimized for 850nm & 980nm

G. Allwood, G. Wild and S. Hinckley, Proceedings of the 19th Australian Institute of Physics (AIP) Congress 2010.

4.2.1. Abstract

We present a new study of power over optical fibre, using silicon-based photovoltaic micro-cells. The thickness of the micro-cells is optimized for incident light of 850nm and 980nm producing efficiencies of up to 43%.

4.2.2. Introduction

Research on III-V material based photovoltaic power converters (PPCs) typically involves complex heterostructures of GaAs or InP, which have shown optical power conversion as high as 50% [1]. However, these types of PPCs are expensive to fabricate, therefore limiting the viability of their use in optical fibre networks. Terrestrial solar cell development for high power applications using silicon-based cells has also indicated high efficiencies for these types of structures under monochromatic illumination [2].

In this paper, we present the results of a study to optimize the power output of a simple silicon-based pn junction photovoltaic micro-cell for monochromatic optical fibre illumination of 850nm and 980nm light. A wavelength of 850nm corresponds specifically to a minimum in the attenuation of standard silica fibres. High power laser light sources are also readily available at 980nm. Hence, optimizing power conversion at these wavelengths would reduce the cost of incorporating these devices into optical fibre networks. Furthermore, modern optical fibre communication networks use long wavelengths such as 1310nm and 1550nm, again because of minimal attenuation in the fibre. As silicon has a cut-off wavelength of 1100nm, silicon PPCs could easily be integrated into these networks in a stacked architecture, as they would be transparent to the communication signals.

4.2.3. Theory

4.2.3.1. Photovoltaic Power Converter

A photovoltaic power converter is basically a pn-junction photodiode operating in photovoltaic mode. Therefore, we are concerned with the behaviour in the fourth quadrant of the device's I-V characteristic, where the device actually generates power. When a photovoltaic device is illuminated with light, electron–hole pairs (carriers) are generated creating a photocurrent. The total current is the photocurrent minus the dark or diode current which is related to the reverse saturation current. The photocurrent is proportional to the generation rate and therefore the incident optical power [3]. The maximum power produced is the point on the I-V curve where the current multiplied by the voltage is at a maximum, and is equated by setting the derivative of the power with respect to the voltage to zero. Fig. 4.2.1 shows the typical I-V and P-V curves of a photovoltaic cell.

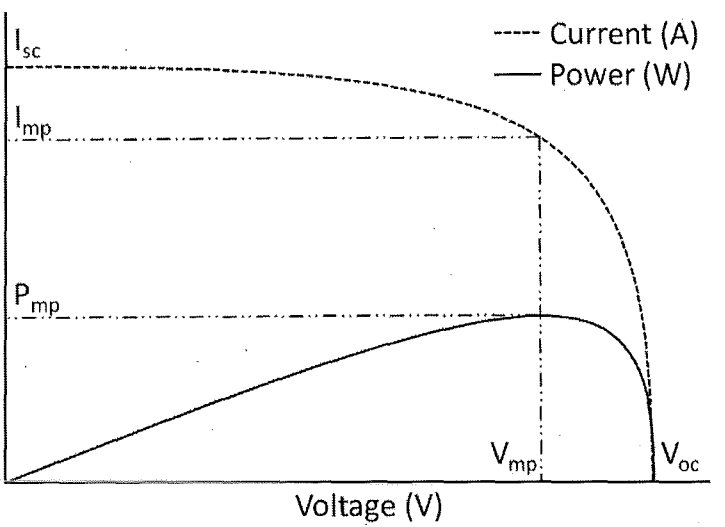

Fig. 4.2.1: I-V and P-V curve of a photovoltaic cell under illumination.

The parameters that define the performance of a solar cell are the short circuit current, I_{SC}, the open-circuit voltage, V_{OC}, and the fill factor, FF. The short circuit current occurs when the load, and therefore the voltage, equals zero and is equivalent to the photocurrent. The open circuit voltage occurs when the resistive load is considered infinite producing no net current and is given by,

$$V_{oc} = \frac{E_g}{q} - \frac{kT}{q} \ln\left(\frac{I_{SC}}{I_{sat}}\right) \quad (4.2.1)$$

where, E_g is the enegy gap, q is the charge and I_{sat} is the reverse saturation current. The fill factor is the ratio of the maximum output power to the product of I_{SC} and V_{OC}.

The doping concentrations within a device are also important factors in determining both the opto-electrical properties and photovoltaic device performance [4]. An understanding of how the relative concentrations of both the n and p regions affect the overall power output of the device is therefore essential in optimizing its efficiency.

There are two main mechanisms that dominate the current flow within a photovoltaic device; drift and diffusion. Drift occurs within depleted regions and is due to the internal electric field which sweeps free carriers out of the region quickly so that almost all the carriers contribute to the photocurrent and recombination is reduced. Diffusion occurs due to a carrier concentration gradient; charged carriers will diffuse from a region of high concentration to one of low concentration. Recombination processes may reduce the effect of diffusion currents depending on the device geometry [4].

4.2.3.2. Properties of Silicon

Silicon is an indirect bandgap material and therefore makes a relatively poor optical material. However, it has a peak responsivity at approximately 850nm, which is particularly advantageous in optical fibre networks as the attenuation at this wavelength is minimal. Moreover, the absorption coefficient is approximately 1000cm^{-1} at this wavelength meaning approximately 99% of the incoming light is absorbed at a depth of approximately 40um. The absorption coefficient at 980nm is approximately 200cm^{-1}, resulting in a required thickness of over 200um for 99% absorption [5].

4.2.3.3. Simulated Device Structure

A 2D finite-element simulation package, SemiCAD DEVICE Version 1.2, was used for all the simulation studies. The device structure simulated, as shown in Fig. 4.2.2, was a standard pn-junction photovoltaic structure on a bulk p-type substrate. The p-region (base) background doping was uniform at $3x10^{17}cm^{-3}$, whilst the n-region (emitter) doping was simulated by using a diffusion profile with a peak concentration of $1x10^{20}cm^{-3}$ reducing to approximately $1x10^{19}cm^{-3}$ at the junction. Such high doping concentrations have been previously shown to maximize power conversion efficiency [6].

The incident beam had a uniform profile and was 500 x 500um with a uniform profile, so as to completely cover the front surface, and kept at 100mW optical power, so that the output electrical power in milliwatts would equate to percentage power efficiency. For simplicity, the front contact was considered completely transparent and therefore non-reflective. The rear contact covered the entire surface and was considered completely opaque.

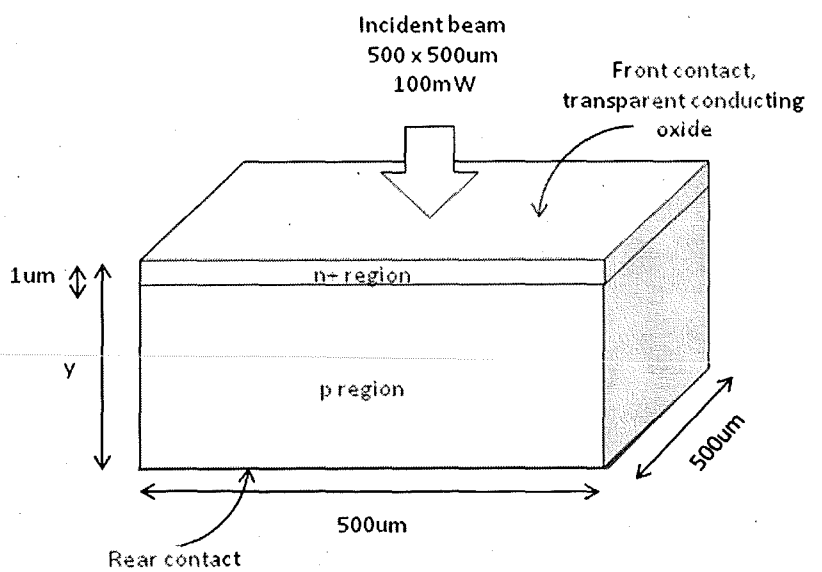

Fig. 4.2.2: Standard device structure used in simulation studies.

4.2.4. Results

Fig. 4.2.3 shows a graph of device thickness against incident wavelength and the corresponding maximum efficiency.

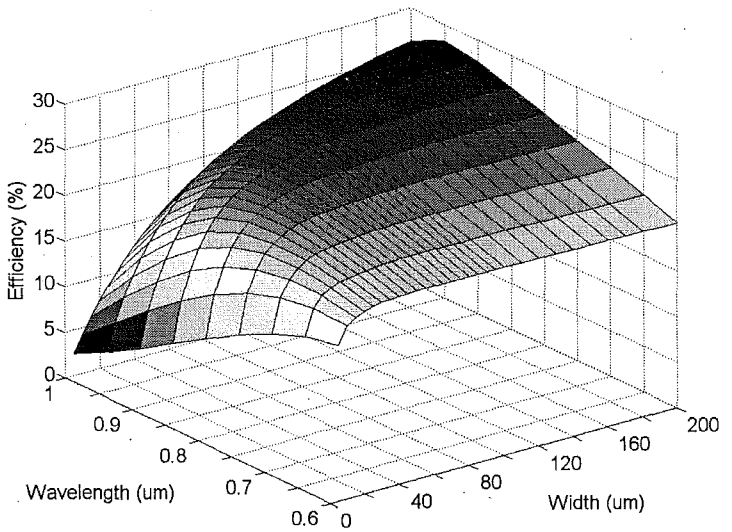

Fig. 4.2.3: Maximum efficiency for device width against wavelength.

The front contact was originally 25um across and located 325um from the left edge so as to similar to a real silicon photodiode. However, it was noted that a standard silicon photodiode structure is by no means optimized for power conversion and hence this type of application.

Fig. 4.2.4 shows a logarithmic plot of wavelength against width. The equation can be used to predict the optimum width for a given wavelength, i.e. the optimum width for a wavelength of 980nm is approximately 265um.

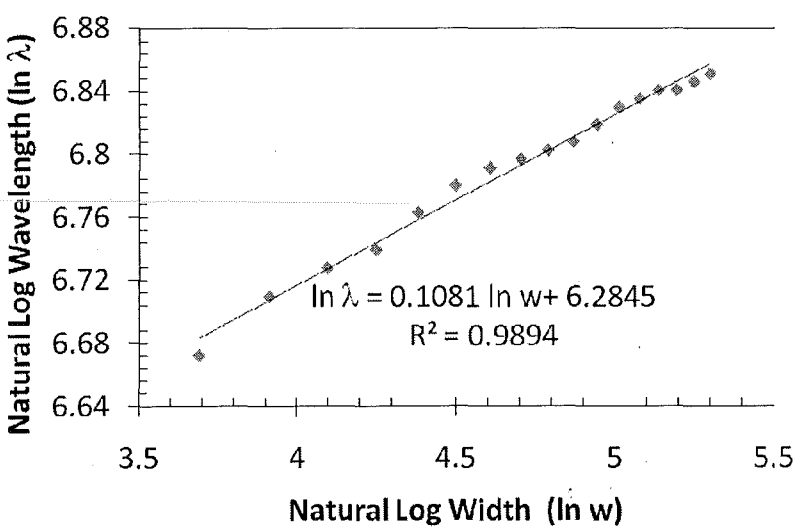

Fig. 4.2.4: Logarithmic graph of wavelength against width.

A consideration was made to increase the size of the front contact such that it was almost the same width as the emitter region. This improved the collection of

carriers considerably and therefore improved the efficiency. Fig. 4.2.5 shows a graph of device width against incident wavelength, and the corresponding maximum efficiency for the improved device.

Fig. 4.2.6 shows the I-V and P-V curves for the device illuminated by 850nm and 980nm at their optimum device width.

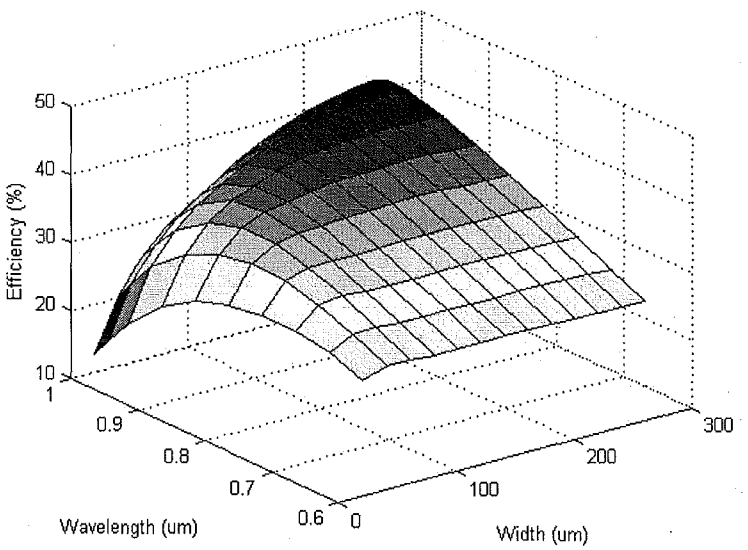

Fig. 4.2.5: Maximum efficiency for device width against wavelength for improved device structure.

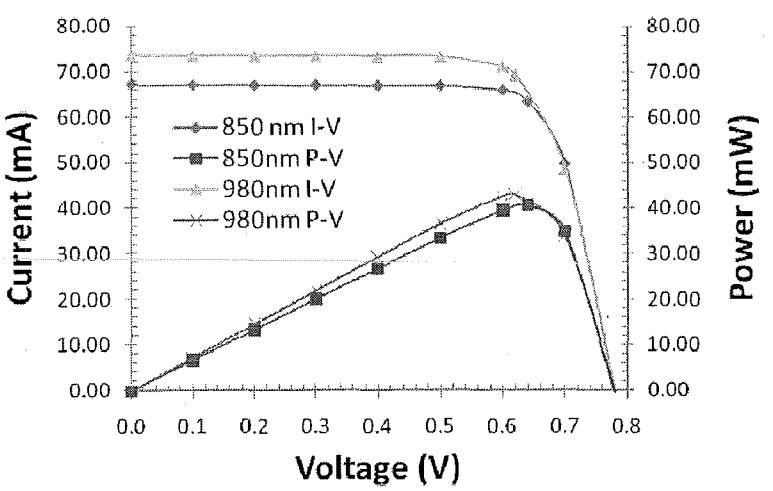

Fig. 4.2.6: I-V and P-V curves for optimum device structures illuminated by 850nm and 980nm light.

Fig. 4.2.7 shows the effect of varying the both the emitter and the base doping concentrations on the output power of the device illuminated by 850nm light.

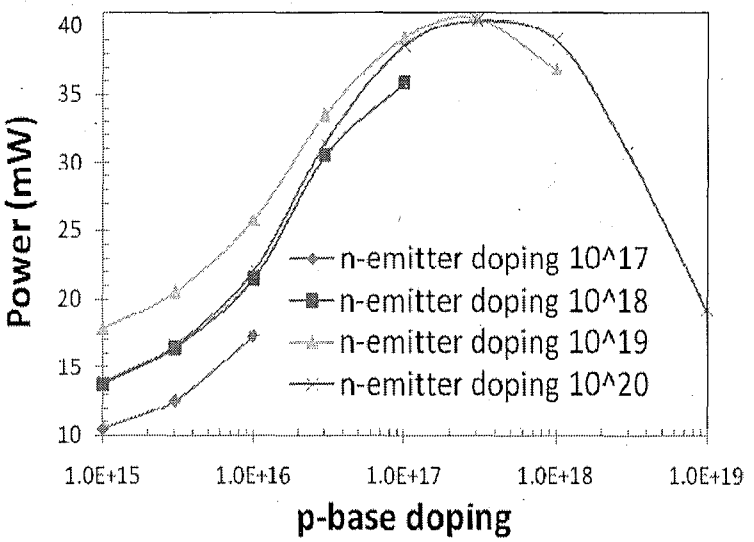

Fig. 4.2.7: Maximum output power for of device illuminated by 850nm light for various emitter and base doping concentrations

Fig. 4.2.8 shows the effect of varying the both the emitter and the base doping concentrations on the output power of the device illuminated by 980nm light.

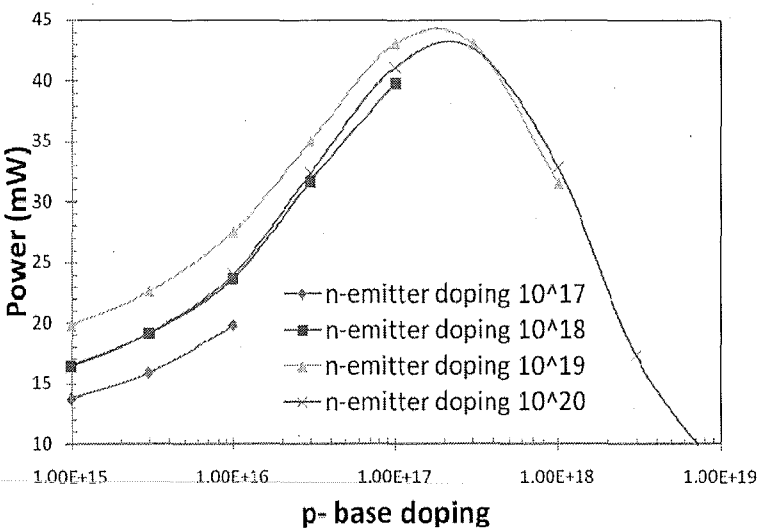

Fig. 4.2.8: Maximum output power for of device illuminated by 980nm light for various emitter and base doping concentrations.

4.2.5. Discussion

By comparing Fig. 3 and Fig. 5, we can see that the geometry of the front contact has a significant effect on the efficiency of a device. In general, the bigger the contact, the better the efficiency as this improves the probability of collection of carriers before they recombine. The solution put forward is to use a transparent

conducting oxide to form an anti-reflective coating. However, a consideration of the increase in cost must be taken into account.

The maximum efficiency of the device illuminated by 850nm light was 40.54% at a width of 180um. The maximum efficiency of this device illuminated by 980nm light was 42.9% at a width of 260um.

The open circuit voltage appears constant, regardless of the wavelength of the illuminating light. This is what we would expect as it is directly related to the bandgap of the material used, in this case silicon. Although a significant increase in short circuit current will reduce V_{oc} from (4.2.1). The longer wavelength light increases the short circuit current as long as the device is thick enough to absorb the maximum amount of light. However, the efficiency of the device does drop off significantly as the wavelength approaches the limit of the bandgap.

These simulations did not take into account the increase in micro-cell resistance with increase in width. However, calculations based on the resistivity of the bulk material with the appropriate carrier concentrations and mobilities only show a reduction in power efficiency of less than 1%. Although It has been shown that significantly increasing the carrier concentrations reduces the mobility of carriers as they experiences more scattering effects.

The doping concentrations of the device were varied to confirm that increasing the doping concentrations resulted in maximum power conversion efficiency. As the doping concentration of the base region increases, and hence the bulk resistivity decreases, the number of minority carriers increases which drift across the junction and contribute to current flow. The increase in base doping concentration causes the short circuit current, I_{SC}, to decrease and the open circuit voltage, V_{OC} to increase until an optimum point is reached. Moreover, there is a limit to the amount of doping in the base region with respect to the doping in the emitter region. As the ratio of the concentrations decrease the diffusion effect is reduced and the size of the depletion region in the emitter increases, resulting in a thinner emitter region, which in turn decreases surface passivation [7]. Moreover, as the doping concentrations increase, Auger recombination becomes more significant and therefore restricts the power conversion efficiency.

4.2.6. Conclusion

Silicon based photovoltaic micro-cells are a cost effective, viable solution for distributed power in optical fibre networks. These results show that these types of simple silicon structures can convert more than 40% of input optical power into output electrical power when illuminated by 850nm and 980nm light.

4.2.7. References

[1] J.G. Werthen, "Powering Next Generation Networks by Laser Light over Fiber," *Optical Fiber Communication Conference and Exposition and The National Fiber Optic Engineers Conference*, February 2008.

[2] M.A. Green, J. Zhao, A.Wang, and S. R. Wenham, "45% Efficient Silicon Photovoltaic Cell Under Monochromatic Light," IEEE Electron Devices Letters, vol. 13, no. 6, pp 317–318, 1992.

[3] S.L. Chuang , *Physics of Optoelectronic Devices*, 1st edition, New York: Wiley, 1995, pp. 597–598.

[4] H.P.D. Lanyon, "The Physics of Heavily Doped N+ P Junction Solar Cells," Solar Cells, Vol. 3, No. 4, pp. 289-311, July 1981.

[5] D.A. Neaman, *Semiconductor Physics and Devices*, 1st edition, McGraw-Hill, New York, New York, 1995, pp. 620-621.

[6] G. Allwood, G. Wild, S. Hinckley, "Photovoltaic Micro-Cell Design for Distributed Power in Smart Sensor Networks" submitted to COMMAD 2010.

[7] J. Brody, A. Rohatgi, V. Yelundur, "Bulk Resistivity Optimized for Low-Bulk-Lifetime Silicon Solar Cells," Progress in Photovoltaics Research and Applications, Vol. 9, 273-285, 2001.

4.3. Power Over Fibre: Material Properties of Homojunction Photovoltaic Micro-Cells

G. Allwood, G. Wild and S. Hinckley, Proceedings of the 6th International Symposium on Electronic Design, Test and Applications (DELTA) 2011.

4.3.1. Abstract

A comparison of the conversion efficiency from optical power to electrical power for three common material homojunction photovoltaic micro-cells was performed. The device widths were varied as a function of incident wavelength such that optimum power conversions were determined whilst under illumination of monochromatic light. GaAs is the most effective material as optimum devices can be fabricated as thin as 15um thick with conversion efficiencies as high as 59%. However, GaAs is extremely expensive and has a limited wavelength response. Although Ge has the lowest conversion efficiency of 36%, it is the only material simulated that is responsive under illumination of long wavelengths above 1.0um, and may be particularly useful for specific applications as it is efficient at both 1310nm and 1550nm, where the attenuation in silica fibres is minimal. Si is a commercially viable material for the use as a photovoltaic power converter (PPC) with conversion efficiencies as high as 43% at 980nm. High power lasers at this wavelength are readily available, as well as the cost of Silicon PPCs being minimal.

4.3.2. Introduction

A completely optical network has many desirable properties. Firstly, the insulating properties of glass and plastic fibres are particularly advantageous in high voltage and strong electromagnetic environments. Secondly, the absence of an electric current also removes many of the problems associated in these situations [1]. Furthermore, the risk of sparks causing an explosion in gaseous environments is eliminated.

High speed communication over optical fibres is now common practice due to many of the advances made in both fibre and laser technology. Optical fibre sensors

(OFSs) are now also being used for a variety of applications, particularly due to their ability to be multiplexed. By utilising a local processor, OFSs can be made intelligent, as with other smart sensors. These processors can then be connected to form a Distributed Optical Fibre Smart Sensor (DOFSS) network [2].

At the network's local level, sensors within a single length of optical fibre could be shared between processors. This optical fibre link then provides the ideal means to share information locally. That is, a DOFSS system would not just utilise OFSs, it would also utilize optical fibre communications. Since there would be a lack of conventional wired links between the nodes of the network, the distribution of power throughout the network must be considered. Since the dedicated optical fibre links exist between nodes for sensing and communication, the ideal solution is then to use these links to distribute power, with power-over-fibre using Photovoltaic Power Converters (PPCs) [3].

In this study, a comparison of different materials for use as PPCs is made and the advantages and disadvantages of each material are discussed. Many of the limiting factors associated with the conversion of optical power to electrical power in terrestrial solar cells are introduced when designing materials for broadband solar illumination. For this reason, the conversion efficiencies of PPCs are typically much higher as they are illuminated by monochromatic light form an optical fibre. Moreover, there are no disadvantageous shading effects.

4.3.3. Theory

4.3.3.1. Photovoltaic Power Converter

A photovoltaic power converter is basically a pn-junction photodiode operating in photovoltaic mode. Therefore, we are concerned with the behaviour in the fourth quadrant of the device's I-V characteristic, where the device actually generates power. When a photovoltaic device is illuminated with light, electron–hole pairs (carriers) are generated creating a photocurrent. The total current is the photocurrent minus the dark or diode current which is related to the reverse saturation current. The photocurrent is proportional to the generation rate and therefore the incident optical power [4]. The maximum power produced is the point on the I-V

curve where the current multiplied by the voltage is at a maximum, and is equated by setting the derivative of the power with respect to the voltage to zero. Fig. 4.3.1 shows the typical I-V and P-V curves of a photovoltaic cell.

The parameters that define the performance of a solar cell are the short circuit current, I_{SC}, the open-circuit voltage, V_{OC}, and the fill factor, FF. The short circuit current occurs when the load, and therefore the voltage, equals zero and is equivalent to the photocurrent. The open circuit voltage occurs when the resistive load is considered infinite producing no net current. The fill factor is the ratio of the maximum output power to the product of I_{SC} and V_{OC}.

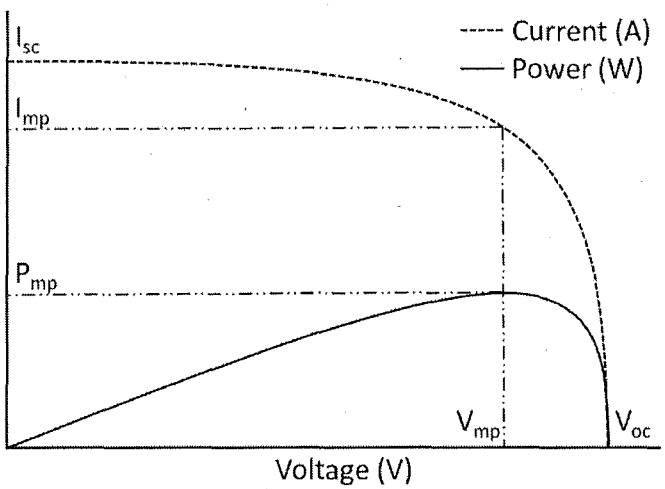

Fig. 4.3.1: I-V and P-V curve of a photovoltaic cell under illumination.

There are two main mechanisms that dominate the current flow within a photovoltaic device; drift and diffusion. Drift occurs within depleted regions and is due to the internal electric field which sweeps free carriers out of the region quickly so that almost all the carriers contribute to the photocurrent and recombination is reduced. Diffusion occurs due to a carrier concentration gradient; charged carriers will diffuse from a region of high concentration to one of low concentration. Recombination processes may reduce the effect of diffusion currents depending on the device geometry [5].

4.3.3.2. Properties of Silicon

Silicon is an indirect bandgap material and therefore makes a relatively poor optical material. However, it has a peak responsivity at approximately 850nm, which

is particularly advantageous in optical fibre networks as the attenuation at this wavelength is minimal. Moreover, it has a 90% absorption rate at a depth of approximately 40um at 850nm [6]. One final advantage of using silicon is that modern optical fibre communication networks use long wavelengths such as 1310nm and 1550nm, because of minimal attenuation in the fibre. As silicon has a cut-off wavelength of 1100nm, silicon devices could easily be integrated into these networks in a stacked architecture, as they would be transparent to the communication signals. Terrestrial solar cell development for high power applications using silicon-based cells has indicated high efficiencies for these types of structures under monochromatic illumination [7].

4.3.3.3. Properties of Germanium

Germanium is also an indirect bandgap material although the energy gap is much lower, just 0.66eV. It is responsive across a large wavelength range from 0.4um to 1.88um. This means it could be used as a PPC in optical networks at 1310nm or 1550nm, again meaning there would be minimal attenuation in the fibre. Furthermore, recent advantages made by the University of Utah, in which a new way of slicing the thin wafers has been developed, may reduce the cost of Ge devices in the future [8].

4.3.3.4. Properties of Gallium Arsenide

GaAs is a direct bandgap material and therefore makes a good optical material. However, it has a limited spectral response from just 0.6um to 0.87um although it still falls within the first window of attenuation minima, 850nm. GaAs has a relatively large bandgap of 1.42eV. Also, the relatively large absorption coefficient means that even highly efficient devices can be very thin. The main disadvantage of GaAs structures is that they are very expensive to fabricate, however, research on III-V material based PPCs, typically using complex heterostructures, have shown optical power conversion as high as 50% [1]. Homojunction GaAs may be slightly cheaper to fabricate, and if the associated efficiencies are still extremely high, it may be a suitable material for specific applications.

4.3.4. Standard Simulated Device

A 2D finite-element simulation package, SemiCAD DEVICE Version 1.2, was used for all the simulation studies. The device structure simulated, as shown in Fig. 4.3.2, was a standard pn-junction photovoltaic structure on a bulk p-type substrate. The p-region (base) background doping was uniform at $3x10^{17}cm^{-3}$, whilst the n-region (emitter) doping was simulated by using a diffusion profile with a peak concentration of $1x10^{20}cm^{-3}$. Such high doping concentrations have been previously shown to maximize power conversion efficiency [9].The incident beam was 500 x 500 um so as to completely cover the front surface and kept at 100mW optical power, so that the output electrical power in milliwatts would equate to percentage power efficiency. For simplicity, the front contact covered the entire surface and was considered completely transparent, and the rear contact covered the entire surface and was considered completely opaque.

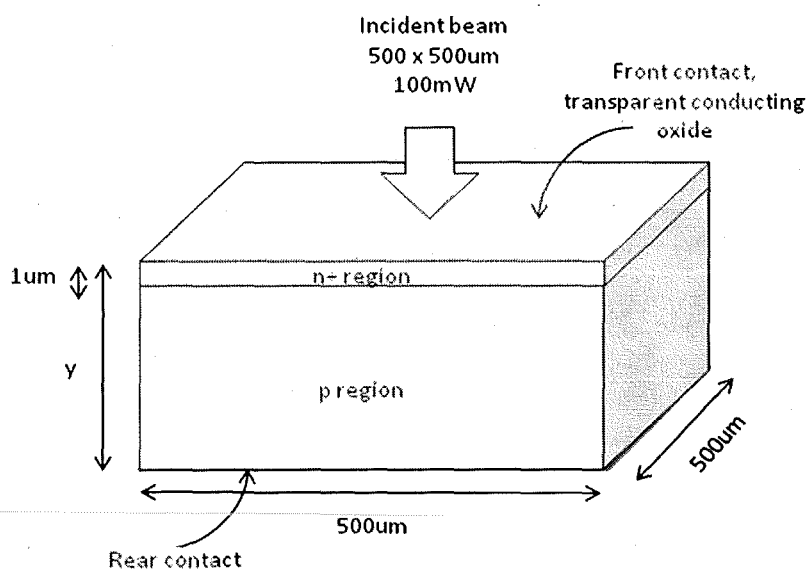

Fig. 4.3.2: Standard device structure used in simulation studies.

4.3.5. Results

Fig. 4.3.3, 4.3.4 and 4.3.5 show graphs of percent power efficiency with respect to wavelength and device thickness, for silicon, germanium and gallium arsenide, respectively.

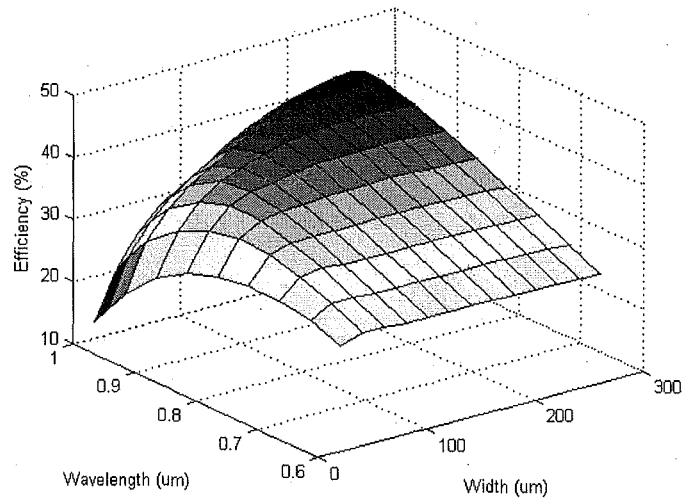

Fig. 4.3.3: Maximum efficiency for Si device thickness against wavelength.

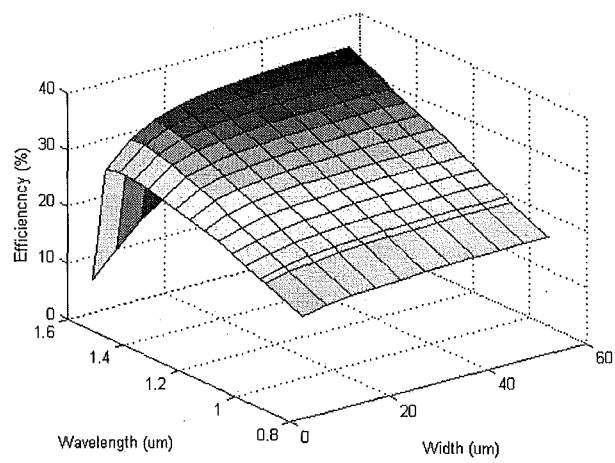

Fig. 4.3.4: Maximum efficiency for Ge device thickness against wavelength.

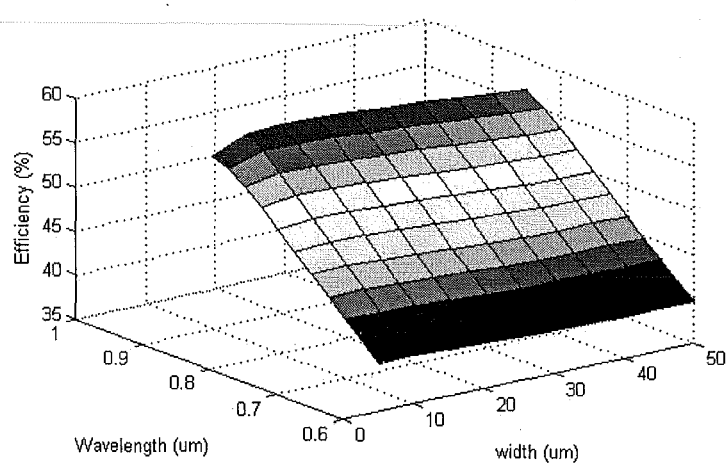

Fig. 4.3.5: Maximum efficiency for GaAs device thickness against wavelength.

Fig. 4.3.6 shows a comparison of the optimum I-V and P-V characteristics of all three devices when illuminated by 850nm light. It is worth noting that the widths of each device are 180, 55 and 15um for Si, Ge and GaAs, respectively.

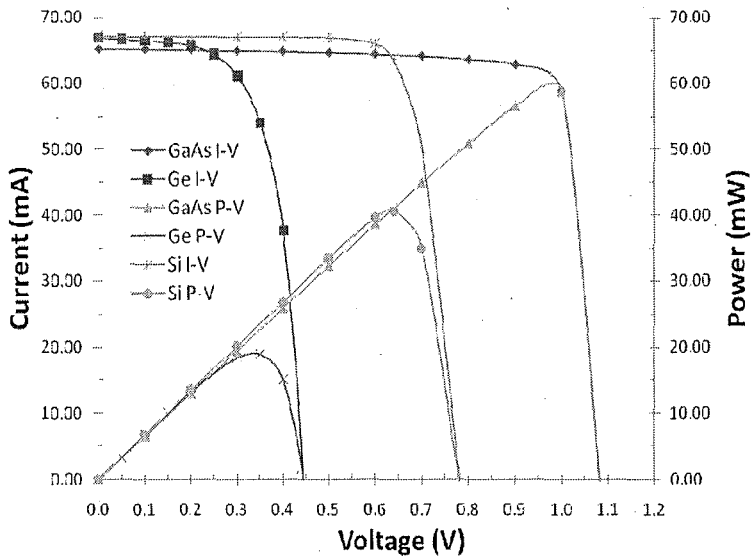

Fig. 4.3.6: I-V and P-V curves for Si, Ge and GaAs photovoltaic cells under illumination of 850nm light.

Fig. 4.3.7 shows a comparison of the silicon and germanium I-V and P-V charcteristics when illuminated by 980nm light. The widths of the devices are 265 and 50um for Si and Ge, respectively.

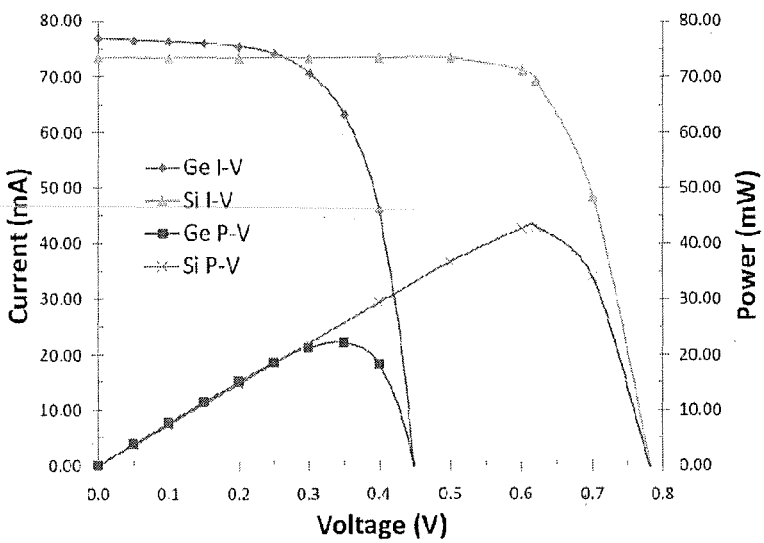

Fig. 4.3.7: I-V and P-V curves for Si & Ge photovoltaic cells under illumination of 980nm light.

Fig. 4.3.8 shows the I-V and P-V characteristics for germanium illuminated by 1310 and 1550nm light. The optimum device thickness was 50um.

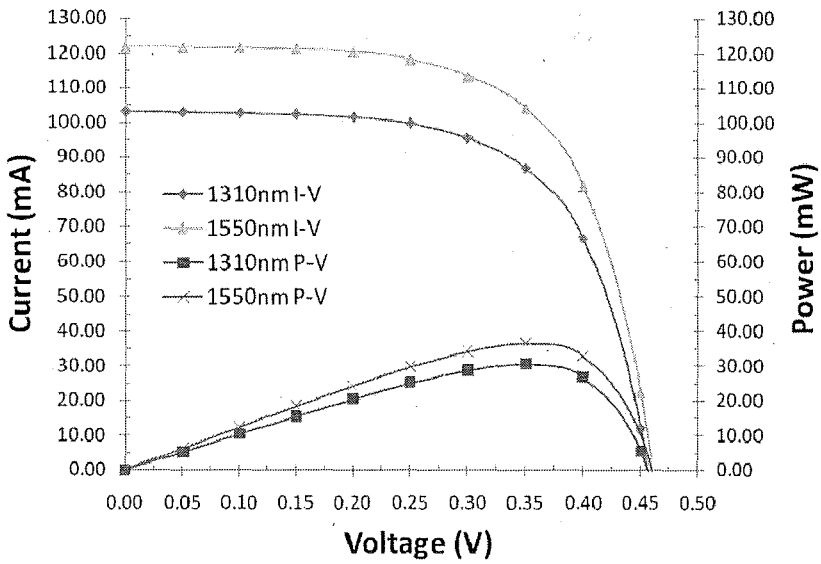

Fig. 4.3.8: I-V and P-V curve of a Ge photovoltaic cell under illumination of 1310nm & 1550nm light.

Table 4.3.1 summerises all of the important results obtained.

Table 4.3.1 simulation results

λ (nm)	material	Width (um)	V_{oc} (V)	I_{sc} (mA)	FF (%)	P_{max} (mW)
850	Si	180	0.77	67.1	78	40.54
	Ge	50	0.45	66.8	63	18.9
	GaAs	15	1.08	65.2	83	58.8
980	Si	260	0.78	73.5	75	42.9
	Ge	50	0.45	76.8	64	22.1
1310	Ge	50	0.46	103.2	64	30.4
1550	Ge	50	0.46	121.8	65	36.4

4.3.6. Discussion

From Fig. 3, 4 and 5 we can see that the efficiencies of all three photovoltaic devices are directly related to the incident wavelength. Optimizing the thickness of each device further improves the efficiency of each device but is not as significant.

Silicon has a peak efficiency of 42.9% at 980nm and a thickness of 260um. Germanium has a peak efficiency of 36.4% at 1550nm and a thickness of 50um. Gallium Arsenide has a peak efficiency of 58.8% at 850nm and a thickness of 15um.

Fig. 6 shows clearly how the I-V characteristics of each device differ when illuminated by 850nm light. The optimum thickness of each device is directly related to the absorption coefficients of each material.

Both Ge and GaAs produce similar, large, short circuit currents. This is because the short circuit current is related to the mobility of minority carrier, holes. The mobility of holes in Ge is approximately 4.5 times greater than the mobility of holes in GaAs, however the thickness of the Ge device is more than 3 times greater, meaning the carriers are more likely to recombine. This tradeoff results in Ge having just slightly greater short circuit current than GaAs. The mobility of holes in Si is similar to that of GaAs, although the optimum thickness is much larger and therefore the carriers are much more likely to recombine.

The open circuit voltage for each device is directly related to the bandgap of the material; the larger the bandgap, the larger the open circuit voltage. The results agree with the general understanding that the open circuit voltage is approximately 70% of the bandgap energy. Hence, even though Ge produces large currents, the peak voltage is too low to generate significant output electrical power, i.e. a large number of micro-cells would need to be connected in series to obtain reasonable supply voltages.

Although GaAs is approximately 50% more efficient than Si at 850nm, Si may still be a viable material for PPC applications at this wavelength, with conversion efficiencies as high as 40% and the obvious low cost of fabrication.

Fig. 7 shows that Si is almost twice as efficient as Ge at 980nm, although the device must be more than 5 times as thick. Again, the low efficiency of power conversion in Ge is due to the low open circuit voltage. Si however, is almost 43% efficient under monochromatic illumination at this wavelength. This agrees strongly with previous work [7]. Furthermore, the peak voltage is approximately 0.6V, meaning an array of 5 micro-cells connected in series would produce 3V, suitable for

powering modern micro-electronic devices, and suggesting that Si maybe an ideal solution for cost effective PPCs. The geometry of multiple cells connected in series was not considered in this study however it has been previously shown that circular segmented device can be coupled effectively to a fibre with the number of segments determining the output voltage.

Fig. 8 shows that Ge is a useful material for use as a PPC at long wavelengths, with maximum power conversion efficiencies of 30.4 % and 36.4% at 1310nm and 1550nm, respectively. The optimum thickness of the device is just 50 um. This means that Ge may be a suitable material for a PPC where size and weight is of great importance, such as devices used by NASA for space exploration. These results also show Ge PPCs could be used for applications in optical networks where the distance between successive repeaters must be maximized.

Table 1 shows the fill factor, FF, is fairly constant for each material, with GaAs having the largest and Ge the lowest. In general, a fill factor of approximately 80% is expected. In this study, Ge has a FF much less than expected. Future considerations may be made in order to improve the FF of Ge and in turn its overall efficiency.

4.3.7. Future Work

This work on power-over-fibre is part of an ongoing research project on distributed optical fibre smart sensor networks. Although this work was primarily focused on showing a comparison between different materials to be used as PPCs, and consistent assumptions were made, future simulations would include less ideal parameters such that the raw data obtained would better reflect the real conversion efficiencies obtainable. Specifically, the geometry of the front contact will be investigated. In addition, the effect of different numbers of series connected devices will be analysed, including the geometry of the overall device.

4.3.8. Conclusion

This research suggests that silicon may be suitable for use as a PPC in DOFSS networks, especially at 980nm where high power lasers are available and cannot be

used with GaAs based devices. As monochromatic light sources were used, much higher efficiencies were expected than for standard solar cells, which have many problems associated with broadband conversion of light to electricity. Although Si devices must be comparatively thick for maximum efficiency, it is common practice to manufacture photodiode cells 300um thick or more. A maximum output efficiency of 40% is predicted for an optimized silicon based photovoltaic micro-cell structure.

This research also confirms the high conversion efficiencies expected from GaAs based devices, however it also outlines the limited applications due to its short wavelength range and the large cost of fabrication. If cost is not of primary concern, GaAs is ideal for producing extremely thin, lightweight and highly efficient PPCs.

Germanium based photovoltaic micro-cells may also show promise in long wavelength applications, especially if the cost of fabrication continues to decrease.

4.3.9. References

[1] J.G. Werthen, "Powering Next Generation Networks by Laser Light over Fiber," *Optical Fiber Communication Conference and Exposition and The National Fiber Optic Engineers Conference*, February 2008.

[2] G. Wild and S. Hinckley, "Distributed Optical Fibre Smart Sensors for Structural Health Monitoring: A Smart Transducer Interface Module," *Proceedings of the Fifth International Conference on Intelligent Sensors Sensor Networks and Information Processing*, 2009

[3] S.J. Wojtczuk, "Long Wavelength Laser Power Converters for Optical Fibers," *Photovoltaic Specialists Conference*, pp. 971-974, September 1997.

[4] S.L. Chuang , *Physics of Optoelectronic Devices*, 1st edition, New York: Wiley, 1995, pp. 597–598.

[5] H.P.D. Lanyon, "The Physics of Heavily Doped N+ P Junction Solar Cells," Solar Cells, Vol. 3, No. 4, pp. 289-311, July 1981.

[6] D.A. Neaman, *Semiconductor Physics and Devices*, 1st edition, McGraw-Hill, New York, New York, 1995, pp. 620-621.

[7] M.A. Green, J. Zhao, A.Wang, and S. R. Wenham, "45% Efficient Silicon Photovoltaic Cell Under Monochromatic Light," IEEE Electron Devices Letters, vol. 13, no. 6, pp 317–318, 1992.

[8] Bamberg, Rakwal, (2008, September 28). Thin Germanium Wafers Shine Bright for Solar Cell Efficiency. Retrieved from http://www.scientificblogging.com/news_releases/thin_germanium_wafers_shine_bright_for_solar_cell_efficiency

[9] G. Allwood, G. Wild, S. Hinckley, "Photovoltaic Micro-Cell Design for Distributed Power in Smart Sensor Networks" submitted to COMMAD 2010

CHAPTER 5

EXPERIMENTAL RESEARCH PAPERS

This chapter includes two papers containing results of various experiments involving photovoltaic cells that have been submitted, peer reviewed and accepted to different conferences within Australia. Each paper has been published in the relevant conference proceedings.

5.1. Power-over-Fibre for Distributed Optical Fibre Smart Sensor Networks

G. Allwood, G. Wild and S. Hinckley, Proceedings of the 35th Australian Conference on Optical Fibre Technology (ACOFT) 2010.

5.1.1. Abstract

This study analyses losses associated with network architectures for power-over-fibre in distributed optical fibre smart sensor networks. We show that multiplexing communication and power signals together does not significantly affect the power generated.

5.1.2. Introduction

A completely optical network has many desirable properties; firstly, the insulating properties of glass and plastic fibres are particularly advantageous in high voltage and strong electromagnetic environments. Secondly, the absence of an electric current also removes many of the problems associated in these situations [1]. Furthermore, the risk of sparks causing an explosion in gaseous environments is eliminated.

High speed communication over optical fibres is now common practice due to many of the advances made in both fibre technology and laser technology. Optical fibre sensors (OFSs) are now also being used for a variety of applications particularly due to their ability to be multiplexed. By utilising a local processor, OFSs can be

made intelligent, as with other smart sensors. These processors can then be connected to form a Distributed Optical Fibre Smart Sensor (DOFSS) network [2].

At the network's local level, sensors within a single length of optical fibre could be shared between processors. This optical fibre link then provides the ideal means to share information locally. That is, a DOFSS system would not just utilise OFSs, it would also utilize optical fibre communications. Since there would be a lack of conventional wired links between the nodes of the network, the distribution of power through the network must be considered. Since the dedicated optical fibre links exist between nodes for sensing and communication, the ideal solution is then to use these links to distribute power, with power-over-fibre using Photovoltaic Power Converters (PPCs) [3].

Research on III-V material based PPCs, typically uses complex heterostructures involving GaAs or InP, and have shown optical power conversion as high as 50% [4]. Terrestrial solar cell development for high power applications using silicon-based cells has also indicated high efficiencies for these types of structures under monochromatic illumination [5].

Here, we suggest a novel idea of coupling a silicon photovoltaic micro-cell to an optical fibre for use as a PPC for power distribution in DOFSS networks. Silicon, although not the most efficient optical power converter, may be suitable for this application because of its high responsivity between 600nm and 900nm, as well as its obvious low cost of fabrication, and ease of integration for system-on-a-chip solutions.

In this paper, we present the results of a study analysing the losses associated with the output power of a photovoltaic micro-cell under monochromatic illumination from an optical fibre, when multiplexed with additional signals. The feasibility of a completely optical network depends entirely on whether the associated losses are minimal. This will have implications on the types of systems, and architectures used in DOFSS networks.

5.1.3. Theory

5.1.3.1. Photovoltaic Power Converter

A photovoltaic power converter is basically a pn-junction photodiode operating in photovoltaic mode. Therefore, we are concerned with the behaviour in the fourth quadrant of the device's I-V characteristic, where the device actually generates power. When a photovoltaic device is illuminated with light, electron–hole pairs (carriers) are generated creating a photocurrent. The total current is the photocurrent minus the dark or diode current which is related to the reverse saturation current. The photocurrent is proportional to the generation rate and therefore the incident optical power [6]. The maximum power produced is the point on the I-V curve where the current multiplied by the voltage is at a maximum and is equated by setting the derivative of the power with respect to the voltage to zero. Fig. 5.1.1 shows the typical I-V and P-V curves of a photovoltaic cell.

The parameters that define the performance of a solar cell are the short circuit current, I_{SC}, the open-circuit voltage, V_{OC}, and the fill factor, FF. The short circuit current occurs when the load, and therefore the voltage, equals zero and is equivalent to the photocurrent. The open circuit voltage occurs when the resistive load is considered infinite producing no net current. The fill factor is the ratio of the maximum output power to the product of I_{SC} and V_{OC}.

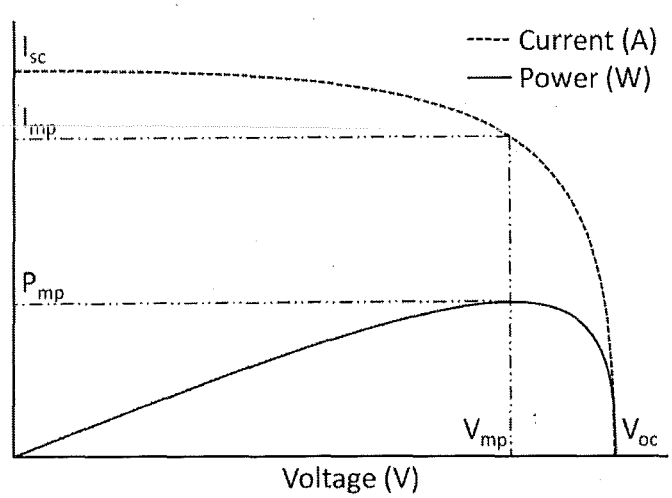

Fig. 5.1.1: I-V and P-V curve of a photovoltaic cell under illumination.

There are two main mechanisms that dominate the current flow within a photovoltaic device; drift and diffusion. Drift occurs within depleted regions and is due to the internal electric field which sweeps free carriers out of the region quickly so that almost all the carriers contribute to the photocurrent and recombination is reduced. Diffusion occurs due to a carrier concentration gradient; charged carriers will diffuse from a region of high concentration to one of low concentration. Recombination processes may reduce the effect of diffusion currents depending on the device geometry [7].

5.1.3.2. Properties of Silicon

Silicon is an indirect bandgap material and therefore makes a relatively poor optical material. However, it has a peak responsivity at approximately 850nm, which is particularly advantageous in optical fibre networks as the attenuation at this wavelength is minimal. Moreover, it has a 90% absorption rate at a depth of approximately 40um at 850nm [8]. One final advantage of using silicon is that modern optical fibre communication networks use long wavelengths such as 1310nm and 1550nm, again because of minimal attenuation in the fibre. As silicon has a cut-off wavelength of 1100nm, silicon devices could easily be integrated into these networks in a stacked architecture, as they would be transparent to the communication signals.

5.1.3.3. Wavelength Division Multiplexing

Germanium is also an indirect bandgap material although the energy gap is much lower, just 0.66eV. It is responsive across a large wavelength range from 0.4um to 1.88um. This means it could be used as a PPC in optical networks at 1310nm or 1550nm, again meaning there would be minimal attenuation in the fibre. Furthermore, recent advantages made by the University of Utah, in which a new way of slicing the thin wafers has been developed, may reduce the cost of Ge devices in the future [8].

5.1.4. Method

First the optical power of the 850nm Laser Diode (LD) was measured using an optical power meter. The LD was biased to its maximum operating current (10mA), using a DC power supply, and a current limiting resistor. This was done for the optical power emitted from the 850nm LD alone, and then through the two Wavelength Division Multiplexing (WDM) couplers.

Following the optical power measurements, electrical power measurements from the PPC were taken. The PPC was connected in series to an ammeter and a decade resistance box (used as the load), and in parallel to a voltmeter. From here the resistance was varied to record the I-V characteristics of the PPC. The resistance was varied logarithmically, and around the peak power point, a finer scale was used. Again this method was used with and without the WDM couplers. When the WDM coupler was used, measurements were taken with both the 1310nm source on and off.

Fig. 5.1.2 shows the experimental setup used. When measuring the optical power, the optical power meter was used in place of the PPC.

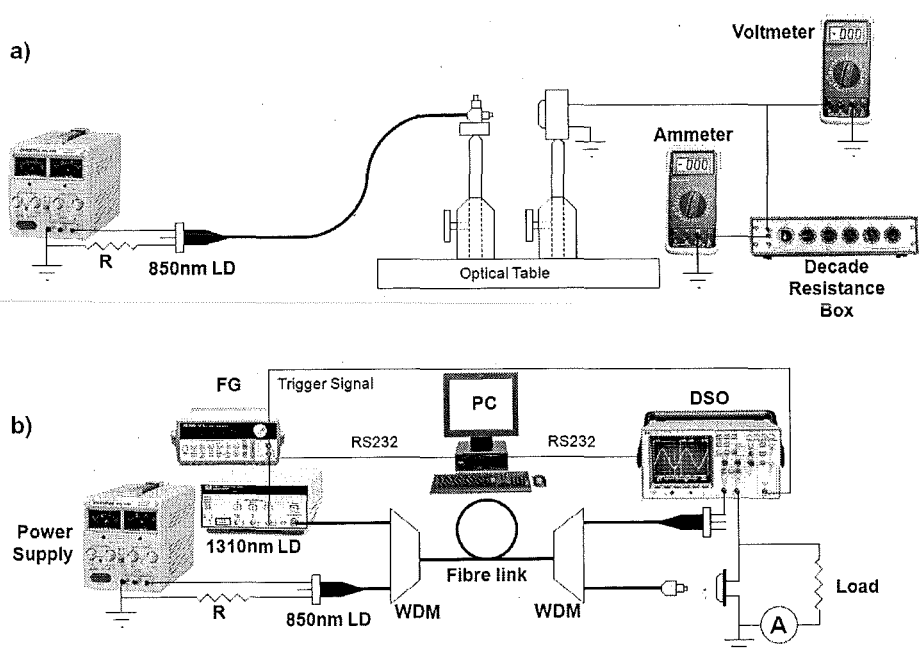

Fig. 5.1.2: Experimental setup used to measure the I-V and P-V characteristics with a) just the 850nm power signal, and b) the 850nm power signal multiplexed with the 1310nm communications signal.

5.1.5. Results

The optical input power before the signal was sent through the WDM filters was recorded as 3.29 mW. After the signal was transmitted through the WDM filters, the optical input power was reduced to 3.14 mW, resulting in a loss of 0.15 mW. Fig. 5.1.3 shows the current-voltage characteristics of a silicon photovoltaic cell under illumination of an 850 nm LD, including the output when multiplexed with and without a 1310 nm LD. Fig. 5.1.4 shows the corresponding power-voltage characteristics. Fig. 5.1.5 shows the output waveforms of the modulated 1310nm communications signal with the 850nm power signal.

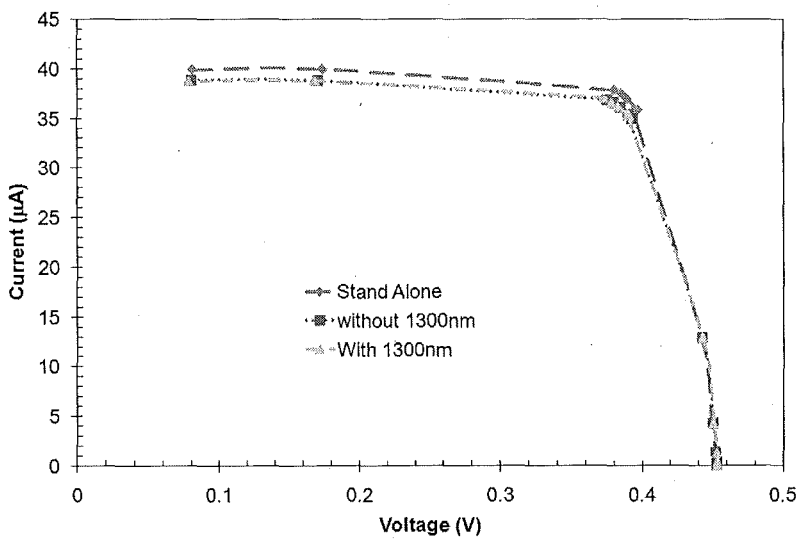

Fig. 5.1.3: I-V curve of power-over-fibre, using just the 850nm LD, the LD with the WDM, and the combined 850nm and 1310nm signal.

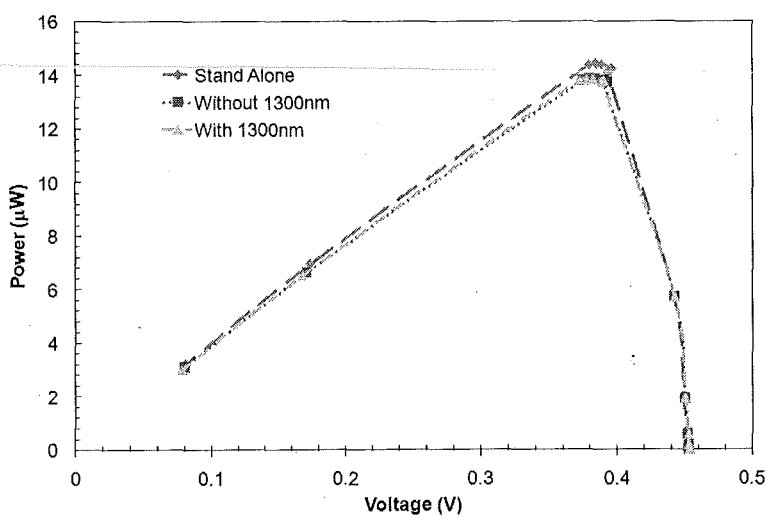

Fig. 5.1.4: P-V curve of power-over-fibre, using just the 850nm LD, the LD with the WDM, and the combined 850nm and 1310nm signal.

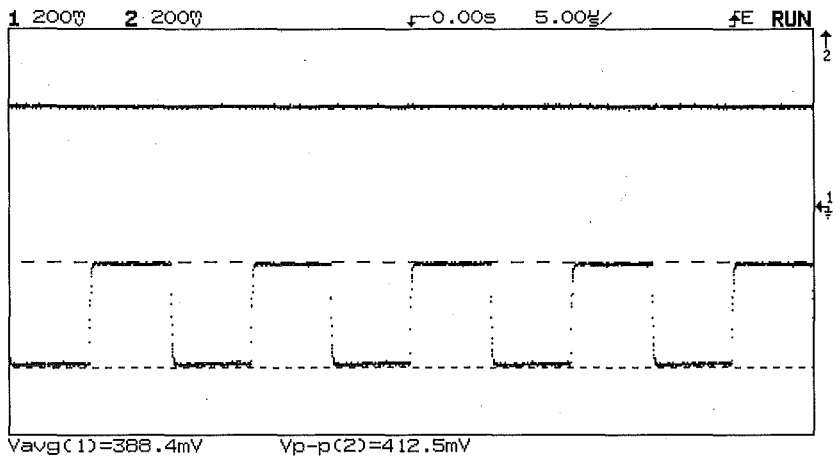

Fig. 5.1.5: Output waveforms of the modulated 1310nm communications signal, (bottom) with the 850nm power signal, (top).

5.1.6. Discussion

5.1.6.1. Findings

The attenuation due to multiplexing a 1310 nm signal with an 850 nm signal given by the manufacturer is 0.2dB per filter, equivalent to a total of 9 percent. Our results show a lower reduction, of approximately 5 percent, in optical power. Fig. 3 and 4 show that the inclusion of a separate signal does not affect the output power of a photovoltaic cell and the only losses that occur are extremely small and are a result of the WDM filters. Fig. 5 confirms there is no interference between an 850 nm power signal and a 1310 nm communication signal. With the use of WDM and circulators, power signals should not be significantly affected by DOFSS network architecture. When signal splitting is needed with intensity splitting components, this should be done before and after the power signal is multiplexed, to avoid the loss of electrical power, which is equivalent to the loss in optical power.

5.1.6.2. Future Work

This work on power-over-fibre is part of an ongoing research project on distributed optical fibre smart sensor networks. Here we took a readily available Si photodiode and used it as a photovoltaic microcell to show the power losses associated with distributing power optically in distributed optical fibre smart sensors networks. In future work, we will be conducting simulations to optimise the use of a Si diode as a photovoltaic microcell. Preliminary results [8], suggest that a

conventional design could easily achieve efficiencies of 25%. Further optimisation looking at monochromatic illumination at 850nm and 980nm could see geometries that increase this further.

5.1.7. Conclusion

In conclusion, we have shown that power efficiency of power-over-fibre will not be significantly affected with the use of WDM in the design of the optical network. The loss in optical power due to the use of the filters, approximately 5%, was equivalent to the observed 5% loss in electrical power produced by the photovoltaic power converter.

5.1.8. References

[1] J. Werthen, "Powering Next Generation Networks by Laser Light over Fiber," *Optical Fiber Communication Conference and Exposition and The National Fiber Optic Engineers Conference*, 2008.

[2] G. Wild and S. Hinckley, "Distributed Optical Fibre Smart Sensors for Structural Health Monitoring: A Smart Transducer Interface Module," *Proceedings of the Fifth International Conference on Intelligent Sensors, Sensor Networks and Information Processing*, 2009

[3] S.J. Wojtczuk, "Long Wavelength Laser Power Converters for Optical Fibers," *Photovoltaic Specialists Conference*, pp. 971-974, September 1997.

[4] J.G. Werthen, "Powering Next Generation Networks by Laser Light over Fiber," *Optical Fiber Communication Conference and Exposition and The National Fiber Optic Engineers Conference*, February 2008.

[5] M.A. Green, J. Zhao, A.Wang, and S. R. Wenham, "45% Efficient Silicon Photovoltaic Cell Under Monochromatic Light," IEEE Electron Devices Letters, vol. 13, no. 6, pp 317–318, 1992.

[6] S.L. Chuang , *Physics of Optoelectronic Devices*, 1st edition, New York: Wiley, 1995, pp. 597–598.

[7] H.P.D. Lanyon, "The Physics of Heavily Doped N+ P Junction Solar Cells," *Solar Cells*, vol. 3, no. 4, pp. 289–311, 1981.

[8] G. Allwood, G. Wild, S. Hinckley, "Photovoltaic cell design for distributed power in optical fibre smart sensor networks," unpublished.

5.2. Distributed Sensing, Communications, and Power in Optical Fibre Smart Sensor Networks for Structural Health Monitoring

G. Wild, G. Allwood and S. Hinckley, Proceedings of the 2010 6th International Conference on Intelligent Sensors, Sensor Networks and Information Processing (ISSNIP).

5.2.1. Abstract

With distributed optical fibre sensors, a single source, a single detector, and a single fibre can be used for up to 1000 fibre Bragg grating sensors. However, this multiplexing architecture is not robust. Damage to any of these individual components can render the entire sensing system useless. To achieve a robust structural health monitoring system, in accordance with NASA's goal of robust or ageless aerospace vehicles, as outlined in the Airframe Structural Integrity and Airframe Airworthiness Programs, Ageless Systems, this type of multiplexing cannot be utilised. To overcome the lack of robustness associated with multiplexing optical fibre sensors together, intelligence along with sensors needs to be distributed around a structure. Distributed Optical Fibre Smarts Sensing (DOFSS) represents a sensing architecture for the structural health monitoring of robust aerospace vehicles. The distribution of intelligence around the structure means that communications and power for the network are a significant consideration. Since optical fibre will be utilised for the sensing, then these "wired" links, can easily be utilised for power. The optical fibre links could also be utilised for the distribution of power around the sensor network. In this work, we investigate the distribution of sensing, communications, and power for DOFSS.

5.2.2. Introduction

As spectral transduction elements, the primary advantage of Fibre Bragg Gratings (FBGs) is seen as their ease of multiplexing. As Optical Fibre Sensors (OFSs), FBGs have several other properties that make them of interest to sensing areas, especially Structural Health Monitoring (SHM) [1]. The most significant of these advantages include reduced size and weight, immunity to electromagnetic

interference, and most significantly, the versatility of FBGs to detect different measurands. For SHM, a FBG system can be used to detect Acoustic Emissions (AEs), actively generated Acousto-Ultrasonic (AU) signals, dynamic strain (e.g. vibration), static strain (e.g. load monitoring), and corrosion, as well as a variety of other measurands.

As with other OFSs, FBGs have found a niche in applications utilizing multiplexing, such as distributed sensing for large scale structures, including bridges and other civil structures. A number of multiplexing architectures can be applied to FBG sensing, including Wavelength Division Multiplexing (WDM) and Time Division Multiplexing (TDM) [2]. However, multiplexed OFSs, with a single fibre, a single source, a single detector, and a single processor, have an inherent flaw, a lack of redundancy. If damage occurs to the structure, resulting in damage to any of the four elements of the system, then potentially the system can become inoperative. Optical Fibre Smart Sensors (OFSSs) represent a robust technology with inbuilt redundancies for both sensors and intelligence. This property goes towards achieving NASA's goal of robust or ageless aerospace vehicles, as outlined in the Airframe Structural Integrity and Airframe Airworthiness Programs [3], Ageless Systems. As with other smart sensors, OFSSs utilise local processing power to add intelligence. The use of a local processor then requires an interface to the OFSs monitored by the processor. To realise OFSSs, a Smart Transducer Interface Module (STIM) was developed [4].

To be effective in SHM, a large number of OFSSs need to be distributed around a structure, that is, Distributed Optical Fibre Smart Sensors (DOFSSs). The use of DOFSSs will enable a smart sensor network to be configured using a large number of STIMs. This will enable a robust SHM system to be realised utilising OFSs. The use of optical fibres in a network suggests that, although against current trends in smart sensing technology [5], the system should be "wired" with the use of optical fibre. The issue of network communications and power distribution then needs to be addressed. Since optical fibres containing sensing elements are required, the use of a fibre optic link between the STIMs means that not only can sensors be shared between processors, increasing redundancy; the links could be used for optical communication and power transmission. That is, DOFSSs could be used to form an all

optical fibre sensor network, linking nodes together for the distribution of sensing, power, and communication, simultaneously. In this work, we demonstrate the multiplexing of optical sensing, communications and power over a single fibre optic link. In addition to this, two STIMs were connected together, via an optical fibre communications link, with one STIM responsible for sensing, and the second STIM responsible for reporting a fault.

5.2.3. Theory

5.2.3.1. Fibre Bragg Grating Sensor

A FBG [6] is a spectrally reflective component that uses the principle of Fresnel reflection. The grating is made up of alternating regions of high and low refractive indices. The periodic grating acts as a filter, reflecting a narrow wavelength range, centred about a peak wavelength. This wavelength, known as the Bragg wavelength (λ_B), is given by

$$\lambda_B = 2n\Lambda, \tag{5.2.1}$$

where n is the average refractive index of the grating and Λ is the grating period.

Any measurand that has the ability to affect either the refractive index or the grating period can be measured using a FBG as a sensor. Specifically, a FBG is sensitive to strain and temperature. The relative change in the Bragg wavelength ($\Delta\lambda_B$) as a function of the applied strain (ε) can then be expressed as,

$$\Delta\lambda_B = \lambda_B\varepsilon\left(1-\frac{n^2}{2}\left[p_{12}-\nu\left(p_{12}+p_{11}\right)\right]\right), \tag{5.2.2}$$

where ν is Poisons' ratio, p_{12} and p_{11} are the strain optic coefficients.

Equation (5.2.2) means that the measurand is encoded onto the wavelength shift of the FBGs. The primary advantage of the absolute nature of wavelength encoding is immunity to optical power fluctuations. However, spectral decoding methods, which are typically slow, cannot be used for very high frequency signals, such as ultrasound. FBGs can also be used as intensiometric sensors, where the sensor

signal is recovered via either power detection, or edge filter detection [7]. Power detection was the first method implemented for FBG sensors to detect high frequency acoustic signals [8]. Fig. 5.2.1 shows the reflectivity as a function of wavelength for a typical FBG.

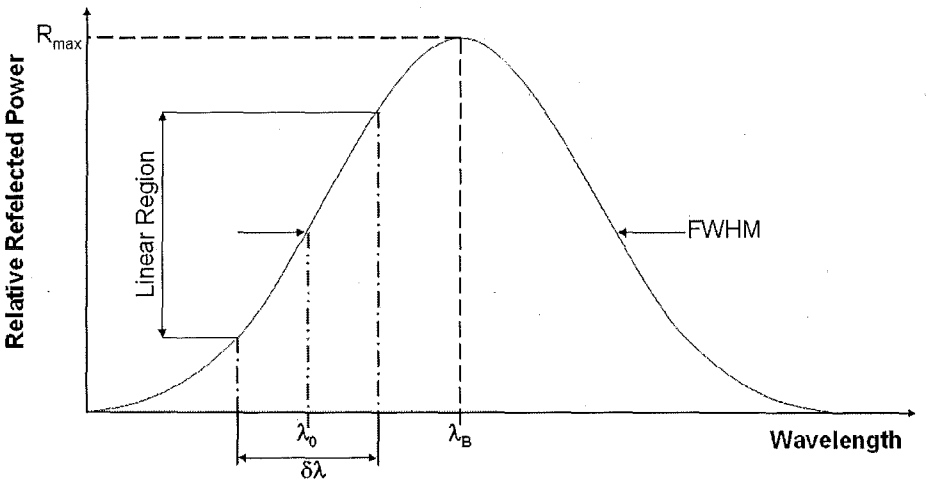

Fig. 5.2.1: The relevant parameters for power detection with a FBG shown on a typical reflectivity plot.

Centred about λ_0, there is a linear region, $\delta\lambda$, between reflectivities of approximately 20 and 80 percent. This linear "edge" of the FBG is used as an optical filter. A narrowband laser source centred about λ_0 is then intensity modulated by the strain induced shift in the wavelength. That is, the reflected optical power is varied as the linear edge of the FBG is shifted in the spectrum. The detection of the signal is then achieved using a simple photoreceiver. The STIM was designed to be directly compatible with edge filter detection, or power detection based intensiometric FBG sensor. Specifically, the STIM was designed for use with a Transmit Reflect Detection System (TRDS) [9], where two photoreceivers and a high speed differential amplifier can be used to monitor dynamic strain signals up to 1 MHz (limited only by the response of the FBG).

5.2.3.2. Photovoltaic Power Converter

A Photovoltaic Power Converter (PPC) is basically a pn-junction photodiode operating in photovoltaic mode. Hence, we are concerned with the behaviour of the device in the fourth quadrant of the I-V curve, where the device actually generates power. When a photovoltaic device is illuminated with light, electron–hole pairs

(carriers) are generated creating a photocurrent. The total current is the photocurrent minus the dark or diode current which is related to the reverse saturation current. The photocurrent is proportional to the generation rate and therefore the incident optical power [10]. The maximum power produced is the point on the I-V curve where the current multiplied by the voltage (the power) is at a maximum. This is given by setting the derivative of the power with respect to the voltage equal to zero. Fig. 5.2.2 shows the typical I-V and P-V curves of a photovoltaic cell.

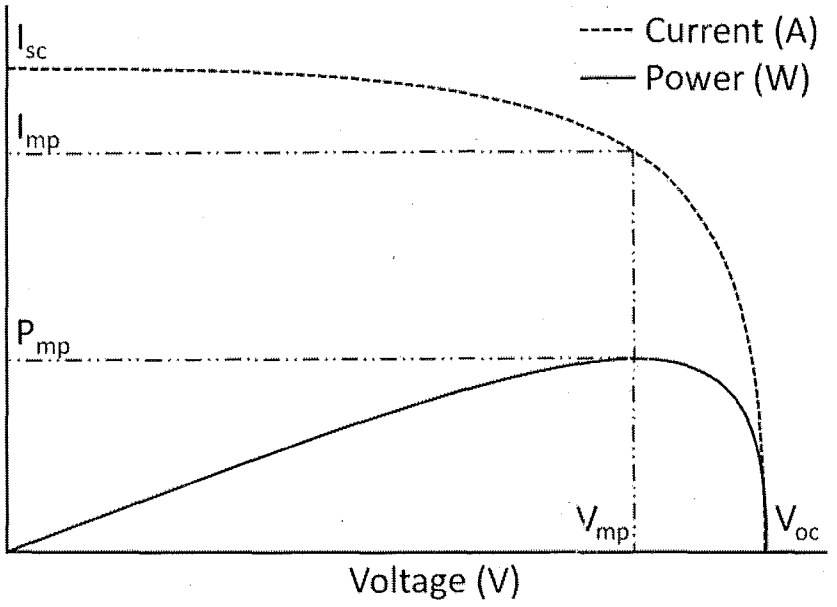

Fig. 5.2.2: I-V and P-V curve of a photovoltaic cell under illumination.

The parameters that define the performance of a photovoltaic cell are the short circuit current (I_{SC}), the open-circuit voltage (V_{OC}), and the fill factor (FF). The short circuit current occurs when the load, and therefore the voltage, equals zero and is equivalent to the photocurrent. The open circuit voltage occurs when the resistive load is considered infinite producing no net current. The fill factor is the ratio of the peak output electrical power to the product of I_{SC} and V_{OC}.

There are two main mechanisms that dominate the current flow within a photovoltaic device; drift and diffusion. Drift occurs within depleted regions and is due to the internal electric field which sweeps free carriers out of the region quickly so that almost all the carriers contribute to the photocurrent and recombination is reduced. Diffusion occurs due to a carrier concentration gradient; charged carriers will diffuse from a region of high concentration to one of low concentration.

Recombination processes may reduce the effect of diffusion currents depending on the device geometry [11].

5.2.3.3. Optical Fibre Communications

Attenuation in optical fibres is an important factor as it ultimately determines the cost of an optical network. If the attenuation is significant then a large number of repeaters are required, resulting in a more expensive network. Attenuation in a silica fibre is a result of both scattering and absorption of the optical signal. Attenuation in an optical fibre can be quantified using,

$$\beta = 10\log\left(\frac{P}{P_0}\right), \tag{5.2.3}$$

where P and P_0 are the output power and input power, respectively. Equation (5.2.3) also gives the loss (in decibels) of power. This could be based on the addition of various photonic components, such as couplers and WDM filters.

5.2.4. Experiments

5.2.4.1. Smart Transducer Interface Module

The Smart Transducer Interface Module (STIM) has previously been reported [4]. It is made up of a TI Digital Signal Processor (DSP), on an eZdsp general purpose evaluation board. The DSP has an onboard 16 channel Analogue to Digital Converter (ADC), capable of sampling the high speed signals for either acoustic sensing, or for communications. The DSP also has available a large number of general purpose I/O.

5.2.4.2. Sensing

The FBG sensor was used as a dynamic strain sensor. The FBG sensor used a transmission based power detection method [12] to convert the wavelength shift of the FBG into an intensity signal for the receiver. A tunable laser (Ando AQ 8201-13B) was used as the source for the power detection, which was directed via the sensing FBG (Broptics GF-1C-1554.13-RX2) to the photoreceiver (Fujitsu FRM3Z231KT). The signal for the receiver was then inverted using an inverting amplifier with a gain

of 1. This was then connected to the ADC for sampling. The first STIM was then used to switch the communications laser, connected to an I/O pin, via a simple transistor switch. The communications signal was then directed to a second receiver which made use of a comparator to convert the communications signal into a TTL compatible digital signal. Fig. 5.2.3 shows the configuration of the STIMs used in the sensing experiments.

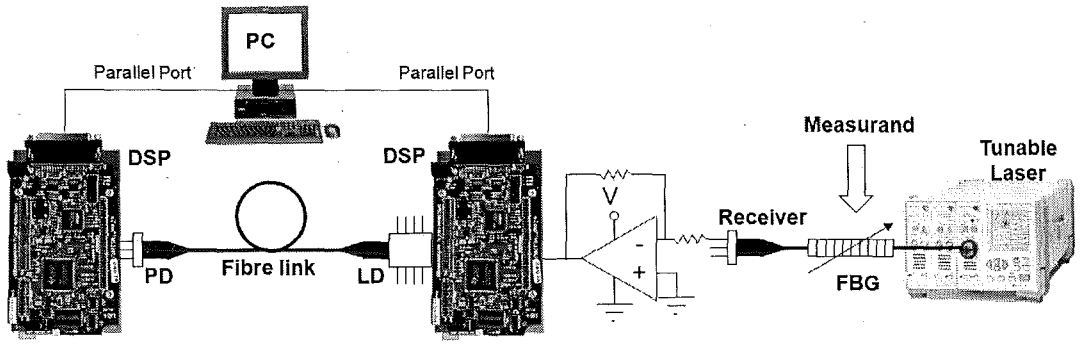

Fig. 5.2.3: Experimental setup for the I-V and P-V characterisation of the silicon photodiode.

5.2.4.3. Power

First the optical power of the 980nm Laser Diode (LD), SDLO-2433-090, was calibrated using the manufacturers supplied data. From here, a measurement was taken using an optical power meter. The LD was biased using an injection current of 14.5mA, from a constant current DC power supply (Goodwill GPS-3030). The voltage of the power supply was set to 1.775 V, the turn on value of the LD. From here, the injection current could then be directly varied with the current adjust dials. The injection current was monitored using an ammeter (Goldstar DM-331).

For the electrical power measurements, the silicon photodiode (Centronic OSD5-5T) was connected in series with an ammeter (Goldstar DM-331) and a decade resistance box (used as the load), and in parallel with a voltmeter (Goldstar DM-331). The resistance was varied logarithmically to generated data for the I-V and P-V curves. To determine the peak power when varying the input optical power, the resistance was varied manually to track the peak power point.

Fig. 5.2.4 shows the experimental setup used to obtain the I-V and P-V characteristics. When measuring the optical power, the optical power meter was used in place of the photodiode.

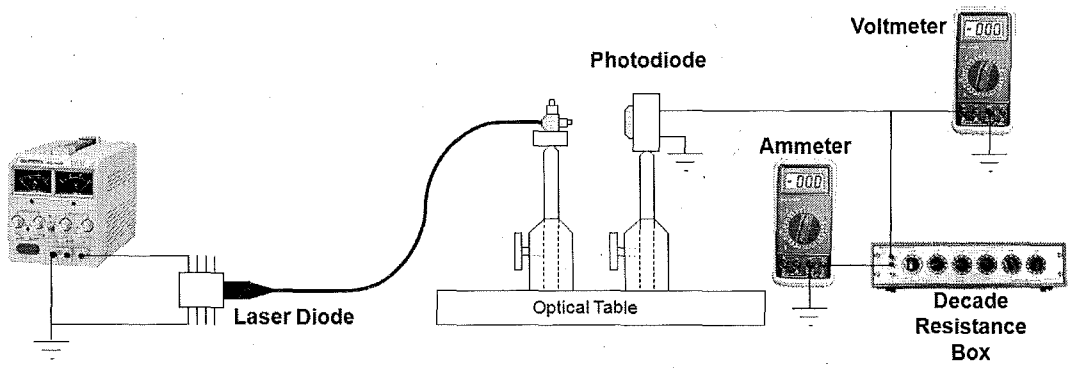

Fig. 5.2.4: Experimental setup for the I-V and P-V characterisation of the silicon photodiode.

5.2.4.4. Multiplexing

To test the use of a single fibre optic link for the simultaneous transmission of optical signals for power, sensing, and communications, a test was performed prior to using the STIM. The experimental setup for this multiplexing experiment is shown in Fig. 5.2.5. The communications signal was generated by On-Off Keying (OOK) a 1552nm laser diode (Mitsubishi LDFU-6275LD-F1) via a simple transistor switch controlled by a function generator (used in place of the digital I/O of the STIM). This was combined with the 1554.13nm tunable laser signal for the sensing via a simple 3dB coupler (Wave Optics 12938). Ideally, a WDM filter should be used to reduce losses. Next the two 1550nm signals were multiplexed with the 980nm laser diode signal (powered by the constant current source as before) via a WDM filter (DP95000102A2222). The FBG sensor was then connected after the WDM filter such that all three optical signals passed through the FBG. After the FBG, the 980nm signal was dropped using a second WDM filter. This was then directed to the silicon photodiode for power generation. The two 1550nm signals were kept together and detected with the same photoreceiver. The combined signals could then be TDM (due to the use of OOK), or they could be filtered in the electrical domain, since the optical communications signals could easily be at frequency greater than 1 MHz, while the frequency of the sensing signals would be less than 1 MHz. The same receiver and inverting amplifier from the sensing experiment was used for the multiplexing experiments. A DSO (Agilent 54600A) was used in place of the ADC of the STIM to display the information.

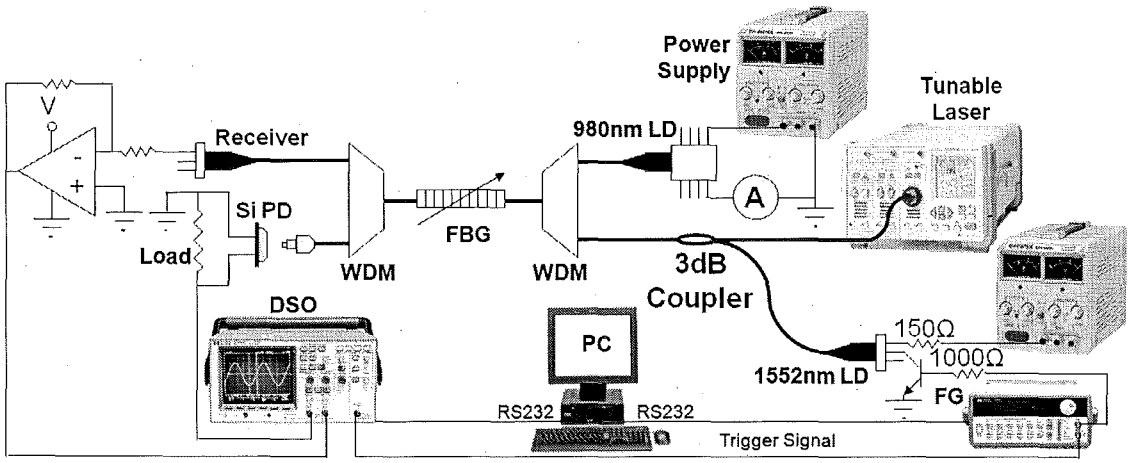

Fig. 5.2.5: Experimental setup for the multiplexing of the power, communications and sensing signals over a single optical fibre link.

5.2.5. Results

5.2.5.1. Power-over-Fibre

Fig. 5.2.6 shows the IV and PV curves for the simple silicon photodiode, illuminated by the 980nm laser diode. The injection current was set to 120mA. The calibration curve to convert the injection current to output optical power (shown in Fig. 5.2.7) gives an optical power of 62mW. Fig. 5.3.8 shows the transfer function, to convert the injection current (directly proportional to the optical power, from Fig. 5.2.7), to output electrical power.

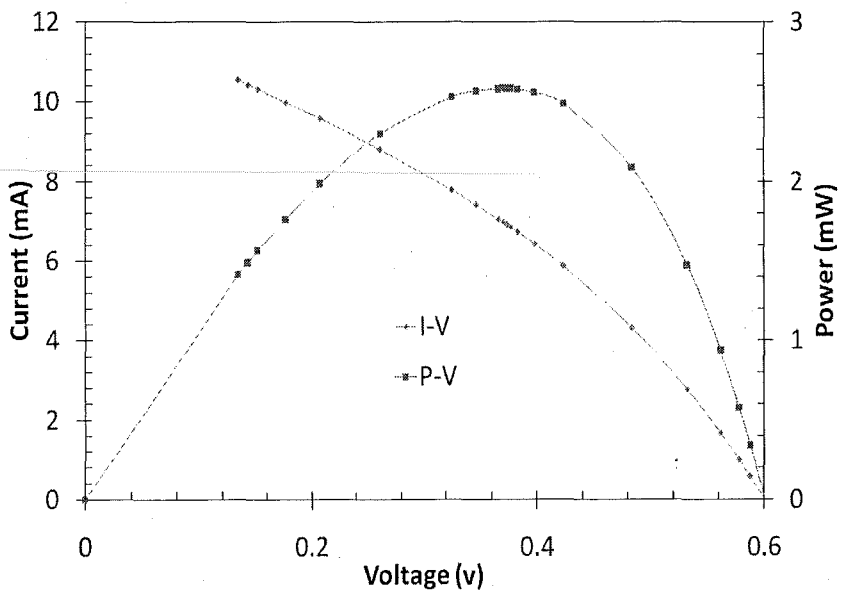

Fig. 5.2.6: I-V and P-V curves of the silicon photodiode with 62mW input power.

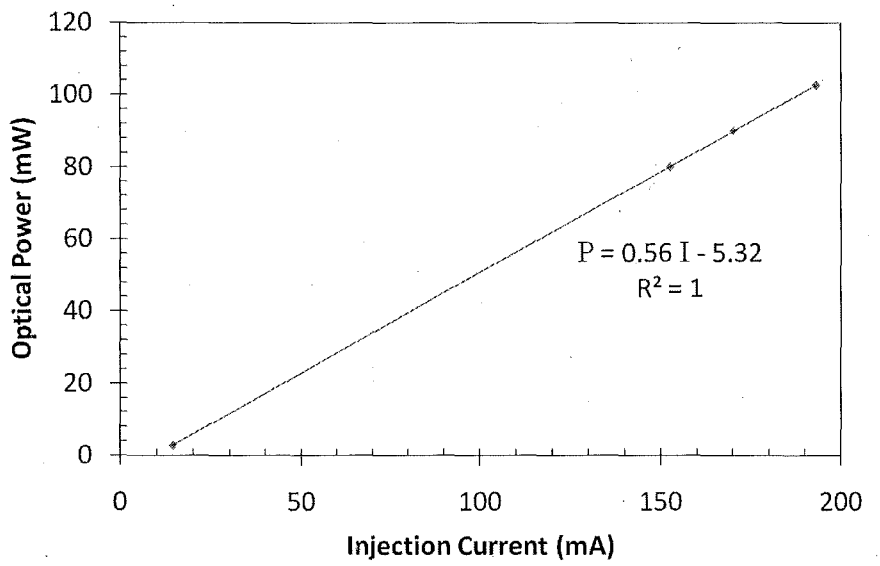

Fig. 5.2.7: Calibration curve to convert the injection current to output optical power for the 980nm laser diode.

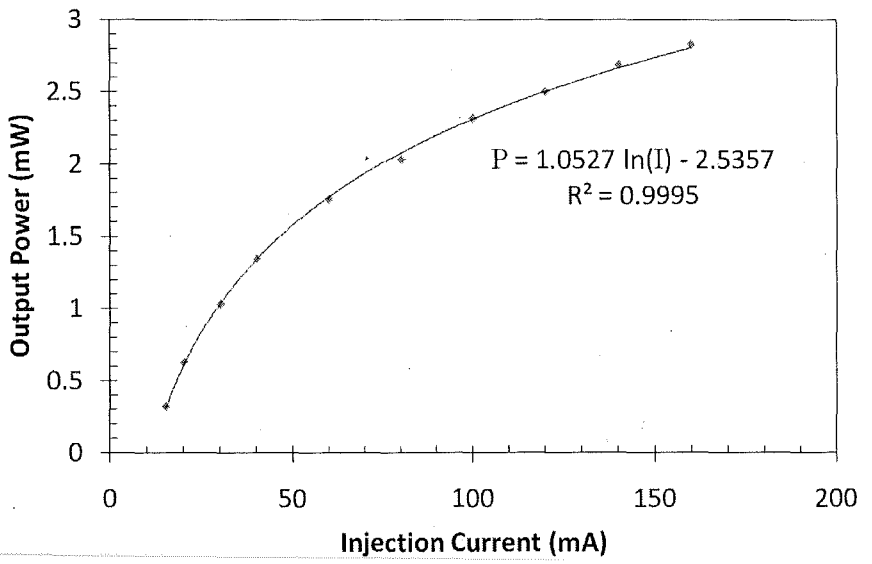

Fig. 5.2.8: The transfer function converting the injection current of the 980nm laser diode into output electrical power of the silicon photodiode.

5.2.5.2. Multiplexing

Fig. 5.2.9 shows the three multiplexed optical signals. This includes the WDM 980nm signal for power-over-fibre, and the TDM 1550nm signals, specifically the 1552nm optical communications signal, and the 1554.13nm optical fibre sensing signal.

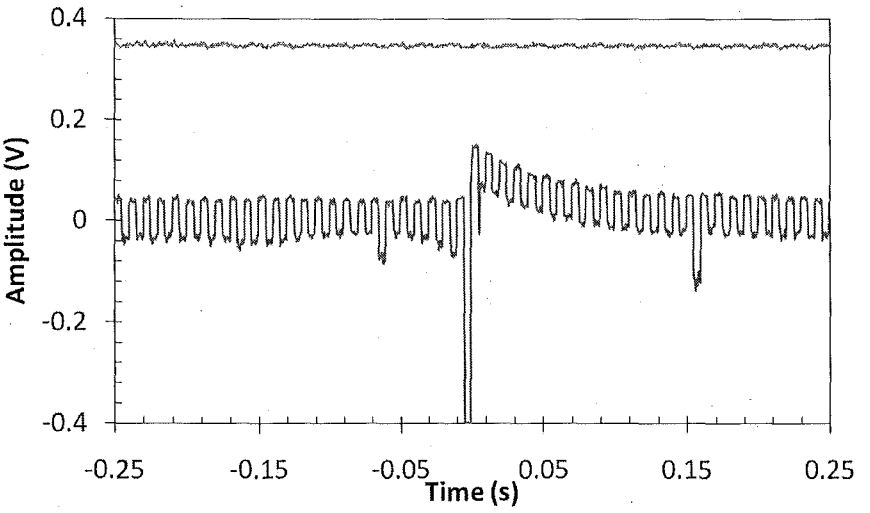

Fig. 5.2.9: The three multiplexed signals. Top, WDM 980nm power signal, and bottom, the TDM 1550nm communications and sensing signals.

5.2.6. Discussion

5.2.6.1. Power-over-Fibre

Fig. 5.2.6 shows a low fill factor, with an approximate short circuit current of 12mA, the theoretical maximum power is then, 7.2mW. With a measured value of 2.6mW, the fill factor is then 36%. Compared with the 62mW of incident optical power, this gives an efficiency of 4%.

The most significant result of the power-over-fibre experiments is the transfer function. The output electrical power appears to be related to the injection current via a logarithmic relationship. That is, as the input optical power is increased, the output electrical power increases at a lower rate. The result of this, combined with a minimum injection current (given as 9.5mA in Fig. 7), is that there is a peak efficiency. This occurs with an injection current of approximately 20mA, or an optical power of 6mW. This gives an efficiency of 10.8%, considerably higher than the 4% with from Fig. 5.2.6. If the laser diode was operated at its maximum optical power of 120mW, then a single PPC would generate approximately 3.2mW of electrical power. However, if this was split in the optical domain, into 20 6mW signals, and converted into electrical power, this would generate 12.96mW of electrical power. That is an increase by a factor of 4. This splitting could be done with an array of PPCs using a single optical fibre, or with optical splitters to separate PPCs via multiple optical fibres.

5.2.6.2. Multiplexing

The results of the multiplexing, shown in Fig. 5.2.9, suggest that TDM can easily be used to combine multiple 1550nm signals. This includes the sensing and communications signals. The impact signal can be easily seen imposed on the OOK digital communications signal. Due to the frequency difference between quasi-static sensing signals, dynamic sensing signals, and communications signals, these three components could also be split by filtering in the electrical domain. Alternatively, the signals could be combined and split using Dense WDM (DWDM) filters. This would require the use of additional receivers, which would also require additional power. The WDM of the power signal with the 1550nm signals also suggests that an all-optical network is viable for the distribution of power and information optically.

5.3.6.3. Future Work

The final stage of the DOFSS work on sensing is the WDM of three FBGs. This is required for both static strain and acoustic sensing. For the acoustic sensing, the multiplexing of three FBGs will enable the source of acoustic emissions to be triangulated. This is important for the localisation of damage in SHM. For the static strain sensing, the multiplexing of three FBGs will enable all of the coefficients of the in-plane strain to be determine, by using the three FBGs as a strain gauge rosette. The current STIM is capable of sampling the WDM signals from the three FBGs, with the use of multiple photoreceivers, by TDM. Fig. 5.2.10 shows the final stage of the DOFSS work, with the fully multiplexed link, connecting two STIMs, for sensing, communications, and power.

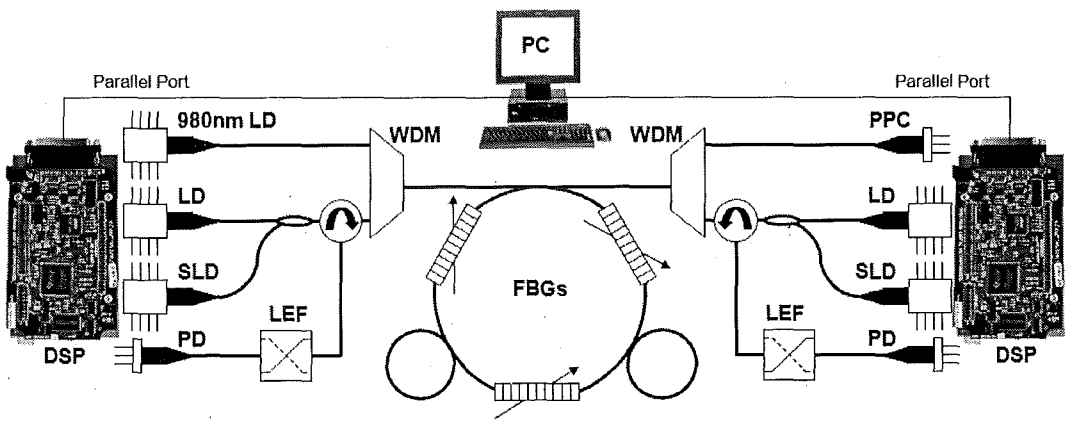

Fig. 5.2.10: Final configuration of DOFSS STIM to STIM connection.

With the successful implementation of WDM for three FBGs for a single STIM, four lots of multiplexed sensors will be cloned. These will be used to monitor in four separate directions. This will require the addition of 3 more STIMs (in addition to the two used in this work). This will give a DOFSS network test bed, which is the final goal of this project.

Coarse WDM (CWDM) could also be used to combine the sensing and communications signals at separate wavelengths. The advantage of this is that the algorithm used for the TDM of the sensing and communications signal would not be required. A power budget would need to look at the advantages and disadvantages associated with TDM and WDM. WDM would result in simpler processing, but requires additional sources and receivers. Alternatively, TDM is more processor intensive; however, it requires fewer optoelectronic components.

Although the efficiency of the PPC reported here is only 10.8% efficient, it is important to note that this is with a silicon photodiode that is not intended for use as a photovoltaic device, or specifically for 980nm. Simulations of a PPC using a simple homojunction structure suggest that when optimised for 980nm, an efficiency of 43% could be achieved [13]. This is comparable to the 45% efficiency of a complex pearl cell previously reported [13]. However, the use of a homojunction would make an array of PPCs easier to fabricate as a system on a chip. Future work will involve the fabrication of a silicon photovoltaic micro-cell optimised for use as a PPC for operation at 980nm.

Future work on the PPC will also confirm the division of the optical power in the optical domain, using multiple silicon photodiodes. This requires the acquisition of a 3dB coupler at 980nm. A similar method will be used, however, the optical power from the 980nm laser will be split between the two silicon photodiodes to confirm that it is more efficient to utilise multiple PPCs.

5.2.7. Conclusion

In conclusion, we have demonstrated the simultaneous transmission of optical signals for power, communications, and sensing, over a fibre optic link for an optical fibre sensor network. The combination of optical signals for sensing and

communications was achieved with time division multiplexing at 1550nm, and the addition of an optical signal for power was achieved with the use of wavelength division multiplexing of 980nm. The sensing and communications signals could easily be decoded in the electrical domain, while the power signal was removed in the optical domain.

The work of distributed power showed a peak power conversion efficiency, measured at 10.8%. This peak efficiency occurred at an optical power of 6mW. With the development of a silicon photodiode specifically for photovoltaic power conversion at 980nm, this efficiency could be significantly improved.

5.3.8. References

[1] R. M. Measures, Structural monitoring with fiber optic technology. San Diego, USA: Academic Press, 2001.

[2] A. D. Kersey, "Multiplexed Bragg grating fiber sensors", in *Proc. LEOS '94*, pp. 153–154, 1994.

[3] E. Generazio (2001) NASA: Meeting of the NDE Communication Group, Materials and Technology (MATTEC) Subcommittee, National Science and Technology Council (NSTC) [Online]. Available: http://www.ntiac.com/mattec/mattec01.html.

[4] G. Wild and S. Hinckley, "Distributed Optical Fibre Smart Sensors for Structural Health Monitoring: A Smart Transducer Interface Module," in *Proc. ISSNIP*, pp. 373-378, 2009.

[5] B. F. Spencer Jr, M. E. Ruiz-Sandoval and N. Kutata, 2004, "Smart sensing technologies: opportunities and challenges", *Structural Control and Health Monitoring*, vol. 11, no. 4, pp. 349–368.

[6] A. Othonos, K. Kalli, *Fiber Bragg Grating. Fundamentals and Applications in Telecommunications and Sensing*. Boston, USA: Artech House, 1999.

[7] B. Lee and Y. Jeong, 2002, "Interrogation Techniques for Fiber Grating Sensors and the Theory of Fiber Gratings", *Fiber Optic Sensors*. New York, USA: Marcel Dekker, pp. 295–381.

[8] D. J. Webb, et al, "Miniature fiber optic ultrasonic probe", in *Proc. SPIE*, vol. 2839, pp. 76–80, 1996.

[9] G. Wild and S. Hinckley, 2008, "A Transmit Reflect Detection System for Fibre Bragg Grating Acoustic Emission and Transmission Sensors", *Lecture Notes in Electrical Engineering - Smart Sensors and Sensing Technology*. Berlin, Germany: Springer, pp. 183–197.

[10] S.L. Chuang, *Physics of Optoelectronic Devices*. New York, USA: Wiley, 1995, pp. 597–598.

[11] H.P.D. Lanyon, "The Physics of Heavily Doped N+ P Junction Solar Cells," *Solar Cells*, vol. 3, no. 4, pp. 289–311, 1981.

[12] N. Takahashi, A. Hirose and S. Takahashi, "Underwater Acoustic Sensor with Fiber Bragg Grating," *Optical Review*, vol. 4, no. 6, pp. 691–694, 1997.

[13] G. Allwood, G. Wild and S. Hinckley, "Photovoltaic Micro-Cell Design for Distributed Power-over-Fibre Optimized for 850nm & 980nm," AIP 2010.

[14] M.A. Green, J. Zhao, A.Wang, and S. R. Wenham, "45% Efficient Silicon Photovoltaic Cell Under Monochromatic Light," IEEE Electron Devices Letters, vol. 13, no. 6, pp 317–318, 1992.

CHAPTER 6

ADDITIONAL RESEARCH

This chapter includes additional research performed on silicon and germanium photodiodes. The results obtained may form the basis of a future journal article or refereed conference paper.

6.1. Silicon illuminated by 850nm light- Optical alignment

The current-voltage characteristics of a silicon photodiode () illuminated by 3.2mW of 850nm light were analysed. Figure 6.1.1 shows that the peak power produced was 0.317mW which equated to a conversion efficiency of 9.78%. This was much higher than the 4% result obtained in section 5.1, because the photodiode used was designed specifically to be responsive to 850nm light, whereas the previous photodiode was not.

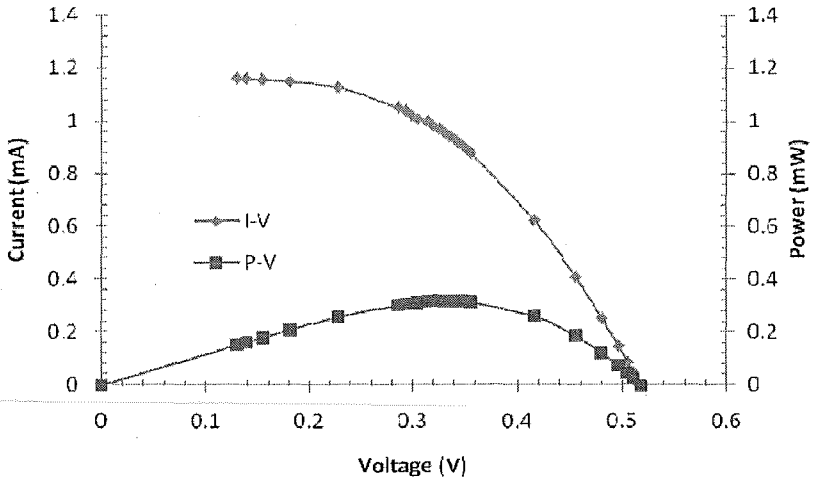

Fig. 6.1.1 I-V and P-V charcteristics of a silicon photodiode illuminated by 850nm light.

The maximum power was then recorded as a function of optical alignment between the fibre tip and the device. The fibre tip was moved in the transverse x-direction, transverse y-direction and in the longitudinal z-direction relative to the device. Figure 6.1.2 shows that the power conversion linearly reduces as a function of longitudinal distance, i.e. the distance from fibre tip to the device.

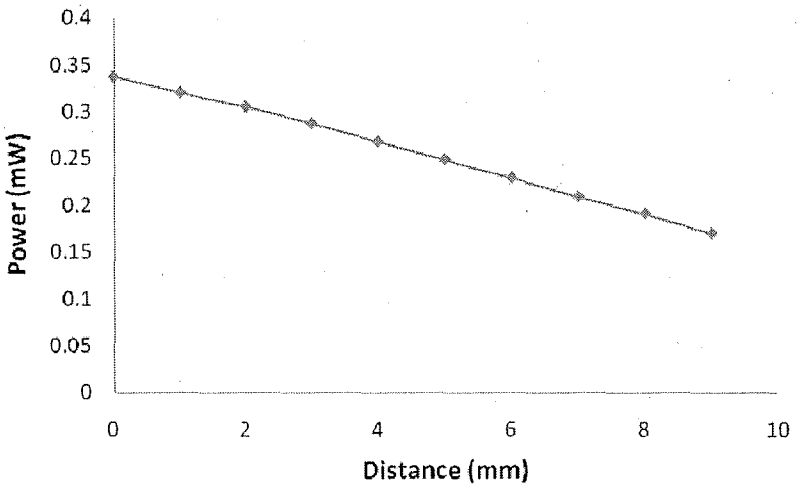

Fig. 6.1.2. Power as a function of longitudinal distance for a silicon photodiode illuminated by 850nm light.

Figure 6.1.3 and 6.1.4 show the output power of the device as a function of transverse x-direction at y=0 and transverse y-direction at x=0. Since both of the curves are not centralised, the results suggest that the optical beam left the fibre at a slight angle. Moreover, the results show that the optical alignment plays a significant role in producing maximum power conversion, as expected. When aligned correctly, the peak power produced was 0.338mW equating to 10% power conversion efficiency.

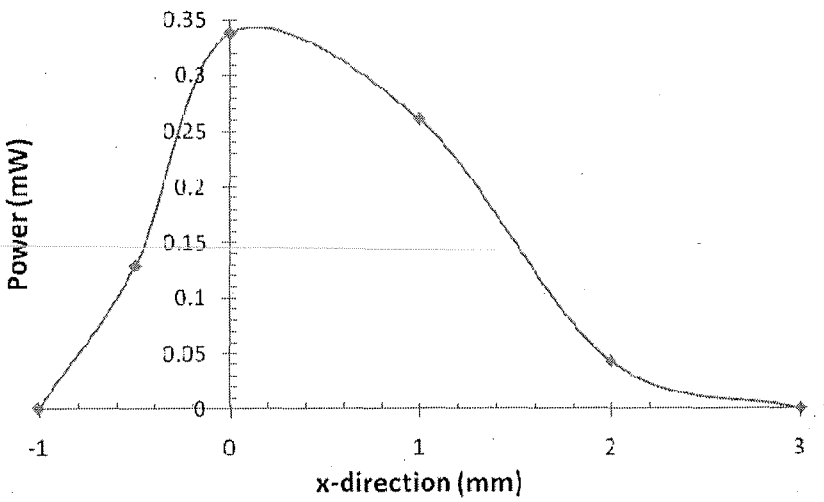

Fig. 6.1.3. Power as a function of transverse x-distance for a silicon photodiode illuminated by 850nm light.

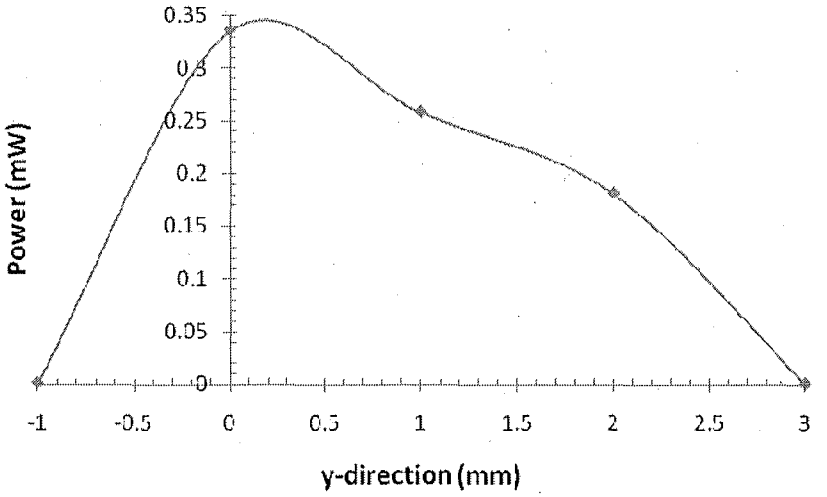

Fig. 6.1.4. Power as a function of transverse y-distance for a silicon photodiode illuminated by 850nm light.

6.2 Germanium illuminated by 1550nm light

Before analysing the output power of a germanium photodiode, a circuit was designed to accurately measure the peak power point. The circuit was connected to PASCO computer interface module (PASCO Scientific 750), and a Data Studio (PASCO Scientific Inc) work sheet was designed to convert the measured voltage signals into the appropriate quantities (i.e. current and power). The use of the software improved the efficiency of collecting results. A variable resistor was used so that a current-voltage sweep could be performed in seconds. Moreover, the Ge photodiode had a fibre optic connection so that the optical coupling was maximised. The circuit is shown in Figure 6.2.1.

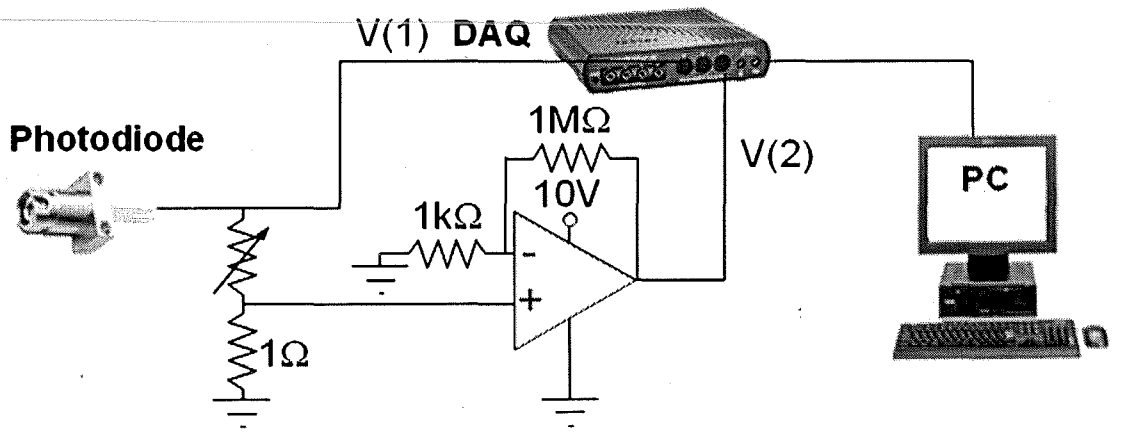

Fig. 6.2.1. Non-inverting circuit for generating I-V and P-V data for a photodiode.

A 1Ω resistor was connected in series with the variable resistor forming a voltage divider. The voltage output of the voltage divider (across the 1Ω resistor) was equal to the current flowing through the series circuit. This relatively small voltage signal (~mV) was amplified using a non-inverting amplifier as shown in the Figure above. A 1kΩ input resistor and a 1MΩ feedback resistor were used, such that the gain would be 1000. V(1) was then the voltage drop across the photodiode and V(2) was the current flow in mA. The P-V curves are shown in Figure 6.2.2.

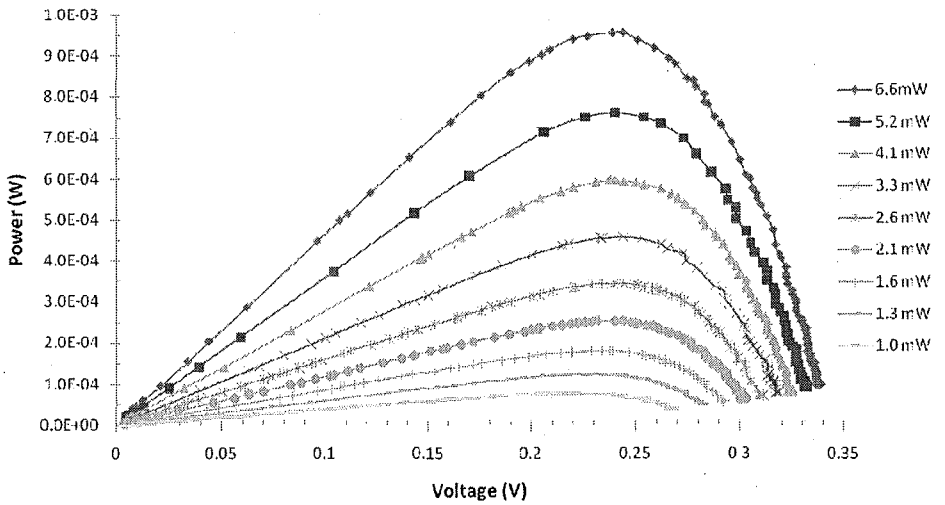

Fig. 6.2.2. P-V curves for a Ge photodiode for various input powers.

The maximum output electrical power recorded was 0.96mW with an input optical power of 6.6mW. This was the maximum input power available from the laser diode used. Larger powers were generated using a SLED (), however the results were not consistant with the manufacturers specifications. Figure 6.2.3 shows a graph of power conversion efficiency as a function of input optical power.

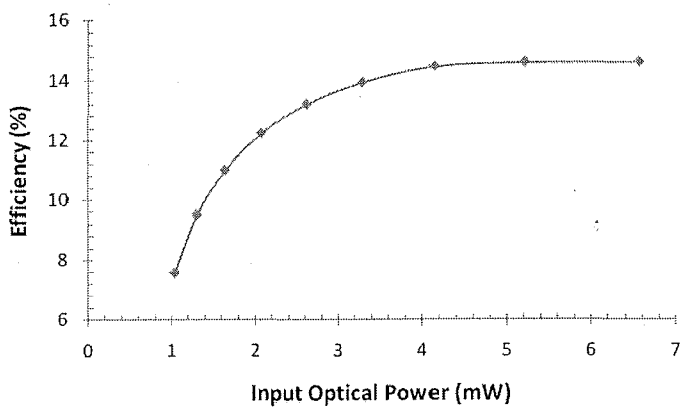

Fig. 6.2.3. Percentage efficiency as a function of inut optical power.

The results suggest there is an optimum input power between 4mW and 7mW producing a maximum efficiency of 14.6%. This results is quite high as the photodiode is not specifically designed for this application. An opimised device illumated by 1550nm light may produce efficiencies similar to the results obtained in Section 4.3.

CHAPTER 7

GENERAL DISCUSSION & CONCLUSION

7.1. Simulations Discussion

SemiCAD DEVICE Version 1.2, like many other software packages used for simulation of semiconductor devices, is a finite element package that uses a drift-diffusion model to solve equations for current densities at given points depending on the relevant variables such as mobility of carriers, temperature, electrostatic potential, etc. From the results obtained from the first three papers, it is clear that there are many factors that affect the output power of a standard photovoltaic device. The most significant factors are detailed below.

Input optical power is directly related to the output electrical power, although this was not explicitly confirmed. Simply by analysing the equations used in the simulations, it is clear that the more optical power that is incident on a device, the more electrical output power is generated. However, there is a lower and upper intensity limit. The lower limit, stemming from the point at which the probability of creating electron-hole pairs is significant enough to generate a current above that of the dark current, and the upper limit arising from heating affects changing the dynamics of the simulations. However, as the primary concern for this thesis is the maximum percentage efficiency of a device, the input power was therefore arbitrary and kept constant at 100mW.

As the drift of carriers is directly related to the electrostatic potential, in which the charged carriers are quickly swept across the depletion region, the efficiency of a device is therefore limited by the diffusion of minority carriers within the bulk region. For this reason, it is clear from the results of section 4.1 that the orientation of the regions plays an important role. Hence, an n+ p device is more efficient than a p+ n device because the mobility of electrons is significantly higher than the mobility of holes.

The incident beam wavelength is perhaps the most significant factor; however, it could be argued that this is not a property of the device itself, although it determines the optimum geometry and structure of the device. As outlined in the theory section,

the effect of the wavelength of the incident beam is restricted by the bandgap of the material used. Silicon based devices are ideal for illumination of both 850nm and 980nm light which produce extremely high power conversion efficiencies, above 40% when the geometry of the device is optimised.

The depth of the device is also dependant on the type of material, specifically the absorption coefficient of the material, which changes depending on the incident wavelength as shown in Figure. 7.1.

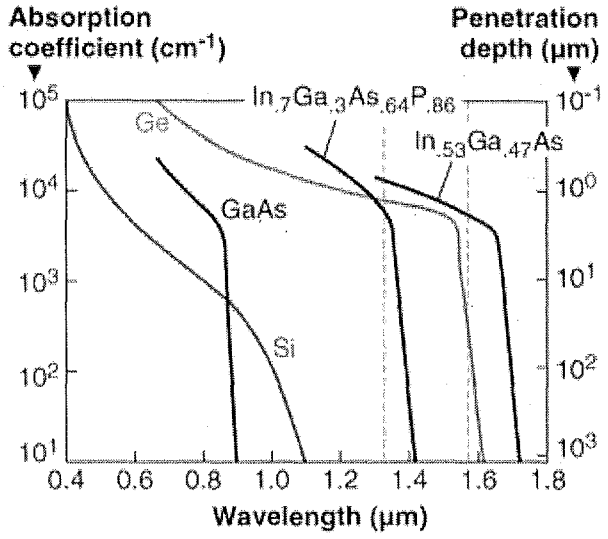

Figure. 7.1. Absorption coefficient for various semiconductors showing penetration depth [1].

The Figure also shows the wavelength range of various materials as the horizontal span of the different curves. As discussed in section 4.3 the depth of a device can be optimised to produce maximum output power for a specific wavelength. For GaAs and Ge, the optimum depths are extremely small. For Si, the device depths are larger, although still well within normal fabricating practices and therefore cheap to produce.

Doping concentrations in each region determine the number of free carriers and the depth of the depletion region, which obviously changes the amount of photocurrent and therefore the power produced. The doping concentration in the bulk region is inversely proportional to the bulk resistivity [2], hence, increasing the doping concentration decreases the resistivity and therefore improves current flow. This agrees with the results obtained which show that increasing the doping concentrations increases the output power of a device. This occurs until the point

where Auger recombination is the dominating process and the efficiency starts to decline. The ratio of the emitter doping concentration to the base doping concentration should also be in the region of 100 so that 99% of the depletion region is in the bulk region.

The position of the front contact also dramatically changes the performance of the device as it determines the amount of carriers that are collected before recombining. SemiCAD Device version 1.2 has some limitations associated with analysing 3D devices as it simulates the device in 2D then multiplies by the third dimension. This means that it is not easy to analyse affectively how the position of the front contact affects the performance of a device as it extends into the third dimension. Moreover, complicated structures tend to take long periods of time to simulate such that, in practice, basic structures were only simulated. However, future research will consist of analysis of more complex design structures.

The results of the silicon device simulations agree very strongly with results obtained by Ortega et al in 2008 [3]. In their simulations, a similar 50um thick device produced 53mA/cm^{-3} current density which equates to approximately 34% power conversion efficiency. A simulation using the same parameters was performed using SemiCAD DEVICE, and yielded an efficiency of 35%, confirming their findings and validating the results obtained in this thesis.

7.2. Experimental Discussion

The experimental results are promising, considering all of the photodiodes used are cheap, off the shelf devices, and the power conversion efficiencies are relatively high. The results are similar to results obtained from simulations of similar devices, therefore it is reasonable to predict that a fabricated device optimised for power conversion may produce similar power conversion efficiencies, up to 43%, as those recorded from the simulations in this thesis.

As expected, there is no significant loss of information when multiplexing multiple signals together and, in fact, the results show a reduction less than the WDM manufacturer's specifications. Optical alignment affects power conversion efficiency

significantly, however it can be easily maximised by using devices with optical fibre connections.

Germanium photovoltaic micro-cells may be an ideal solution for powering remote microelectronics that are a long distance from the source using long wavelength light. Simple silicon structures may be used as an extremely cheap option for powering microelectronics in existing optical fibre networks.

7.3. Future Work

Further research needs to be performed to eliminate some of the problems associated with fabricating cheap transparent front contacts and physically obtaining efficiencies as high as those simulated. In the future, it would be desirable to manufacture a silicon photovoltaic micro-cell in order to test some of the results from the simulations performed in this thesis.

7.4. Conclusion

Power-over-fibre using silicon based photovoltaic micro-cells is a viable cost effective solution for powering microelectronic devices in optical networks. The photovoltaic micro-cells can be implemented into any existing fibre optic network for powering distributed sensors or remote systems, eliminating the need for traditional wired links. Furthermore, this technology, as outlined earlier, has many advantageous properties in extreme environments where conventional electrical power is not possible.

The power conversion efficiency results obtained in this thesis are certainly high enough to warrant further research, development and fabrication of this type of photovoltaic micro-cell. Whilst GaAs-based devices still produce far greater conversion efficiencies, the cost of fabrication limits the possibility of wide scale commercial use. Ge based devices show promise in long wavelength applications and may be used much more in the future as cheaper lasers producing light in the second and third window regime are designed, and the cost of fabrication decreases.

7.5. References

[1] M. Morse, "Semiconductor Detectors: Germanium on silicon approaches III-V semiconductors in performance" laser-focus-world, vol. 43 no. 5, May 2007.

[2] S. M. Sze, *Semiconductor Devices*, *Physics and Technology*, Murray Hill, New Jersey, Wiley, 1985, pp. 38-39.

[3] P. Ortega, S. Bermejo, L. Castener, "High Voltage Photovoltaiv Mini-Modules", Progress in Photovoltaics: Research and Applications, Vol 16, pp 369-377, Wiley, 2009.

APPENDICIES

I - Simulation Package

SemiCAD Device version 1.2 is a finite element package. The semiconductor devices are governed by the follow three equations: Poisson's equation solves for the electrostatic potential ψ and is given by

$$\nabla(\varepsilon \cdot \nabla\psi) = q\left[n - p + \sum(N_A - N_D + N_{AA} - N_{DD})\right]$$

where ε is the permittivity, q is the electronic charge, N_A and N_D are the concentration of ionised acceptors and donors, N_{AA} and N_{DD} are the concentration of ionised acceptor-like and donor-like traps, respectively.

The current continuity equations solve for the electron and hole concentrations, n and p, and are given by

$$\frac{\partial n}{\partial t} = \frac{1}{q}\nabla \cdot J_n + G_n - R_n$$

$$\frac{\partial p}{\partial t} = \frac{1}{q}\nabla \cdot J_p + G_p - R_p$$

where G_n and G_p are the generation rates in $cm^{-3}s^{-1}$ for electrons and holes, R_n and R_p are the recombination rate in $cm^{-3}s^{-1}$ for electrons and holes, respectively. The electron and hole current densities, J_n and J_p are calculated based on the drift-diffusion model:

$$J_n = qn\mu_n\xi_n + qD_n\nabla_n$$

$$J_p = qn\mu_p\xi_p + qD_p\nabla_p$$

The electron and hole mobilities, μ_n and μ_p, are related to the electron and hole diffusion constants, D_n and D_p, through the Einstein relations:

$$D_n = \frac{kT}{q}\mu_n$$

$$D_p = \frac{kT}{q}\mu_p$$

The following quasi-electric field vectors are used in the drift diffusion equations

$$\xi_n = -\nabla\left[\psi + \frac{1}{q}\left(kT\ln N_C + kTin\gamma_n + \chi + \Delta E_C\right)\right]$$

$$\xi_p = -\nabla\left[\psi + \frac{1}{q}\left(-kT\ln N_V - kTin\gamma_P + \chi + E_G + \Delta E_V\right)\right]$$

which account for any spatial variations in the material composition and the band parameters. N_C and N_V are the effective density-of-states for the conduction and valence bands, χ is the electron affinity, E_G is the bandgap energy, and ΔE_C and ΔE_V are the offsets in the conduction and the valence band due to bandgap narrowing. The factors γ_n and γ_p are the ratios of the Fermi-Dirac integrals, but are not used in these simulations.

In order to run a simulation a device file and a run file must be created. An example device file is given below

```
/*
 * ---------------- SEMICAD DEVICE Simulation Example ----------------------
 *                        Dawn Technologies, Inc.
 * file      : Si_diode6.dev
 * device    : silicon diode with 2D implanted doping profile
 *02/05/10
 * ------------------------------------------------------------------------
 */
#library "Silicon.lib"
#library "Insulator.lib"


device diode{
        width  = 500.0;
        orders = 500;  /* gridding parameter */
        maxDx  = 10;
        maxDy  = 5;

        region bulk{
                material    = &bip_silicon;
                optics = &Si_optics;
                srh = "true";
                auger = "true";
                temperature = 300;
                coordinates = {{0.0, 0.0}, {500.0, 0.0},
                               {500.0, 50.0}, {0.0, 50.0}};
                surface{
                        reflect = 0.0;
                        coordinates = {{0.0, 0.0}, {500.0, 0.0}};
        }
                surface{
                        reflect = 1.0;
                        coordinates = {{0.0, 50.0}, {500.0, 50.0}};
        }
        }
```

```
/*
 * electrodes
 */
        boundary cathode{
                type = "ohmic";
                coordinates = {{100.0, 0.0}, {400.0, 0.0}}
        }
        boundary anode{
                type = "ohmic";
                coordinates = {{0.0, 50.0}, {500.0, 50.0}}
        }
/*
 * doping profiles
 */
        profile p_background {
                species = &B_Si;
                field uniform {
                        multiplier = 3.0e17;
                }
        }
        profile n_implant {
                species = &As_Si;
                field n_implant_field {
                        multiplier = 1.0e20;


                        analytic y_profile {
                                argument = "y";
                                type = "diffusion";
                                m0    = 0.5; /* projected range */
                                m1    = 0.25; /* straggle        */
                                m2    = 0.0; /* left  edge of mask opening */
                                m3    = 500.0; /* right edge of mask opening */
                        }
                }
        }

/*
 * beam properties
 */

        beam laser {
                x = 250;
                y = 0;
                angle = 90;
                lambdas = {0.85};
                powers = {1e-1};

                rays = 1;
                reflections = 1;

                field lightarea {
                        analytic spot {
                                argument = "x";
                                domain size {
                                        min = -250;
                                        max = +250;
                                }
                        }
                }
        }

};
```

The device file, as you would expect, defines all of the parameters attributed to the device itself as well as some of the beam parameters.

An example run file is given below

```
/* ----------------------------------------
 * simple dc characteristics of a diode
 * ----------------------------------------
 */
#include "Si_diode6.dev"

main()
{
        ShowProgress = "true";
        outf = "Si_diode6_iv_500.dat";
        rewrite(outf);

        vstart  = 0.3;
        vinc    = 0.05;
        vstop   = 0.8;

        printf("  V(V)          I(A)          P(W)\n");
        nprintf(outf, "  V(V)          I(A)          P(W)\n");

        beamsize = 250;
        min1 = -1*beamsize;
        max1 = beamsize;
        diode.laser.lightarea.spot.size.min = min1;
        diode.laser.lightarea.spot.size.max = max1;


        for (v = vstart; v<= vstop; v += vinc){

                diode.anode.bias = v;
                ia = diode.anode.current;
                p = ia*v;

        printf(" %6.3f      %10.3e       %8.3e\n", v, ia, p);
        nprintf(outf," %6.3f      %10.3e %8.3e\n", v, ia, p);

        /* save two device object snaphots */
                if (v == 0.0) save("Si_diode5.obj.100", &diode);
        }
        printf("Execution Time %g (sec)\n", ExecTime);
}
```

The run file defines what parameters are to be recorded and how often, such as at what voltage and what dopant levels should a measurement be taken and in what increments.